Bioorganic Chemistry 114 (2021) 105137

Contents lists available at ScienceDirect

Bioorganic Chemistry

journal homepage: www.elsevier.com/locate/bioorg

Novel thienopyrimidine-aminothiazole hybrids: Design, synthesis, antimicrobial screening, anticancer activity, effects on cell cycle profile, caspase-3 mediated apoptosis and VEGFR-2 inhibition

Yara El-Dash [a], Emad Elzayat [b], Amr M. Abdou [c], Rasha A. Hassan [a,*]

[a] Pharmaceutical Organic Chemistry Department, Faculty of Pharmacy, Cairo University, Cairo 11562, Egypt
[b] Zoology Department, Faculty of Science, Cairo University, Cairo, Egypt
[c] Microbiology and Immunology Department, National Research Centre, Giza, Dokki 12622, Egypt

ARTICLE INFO

Keywords:
Thienopyrimidine
Aminothiazole
Synthesis
Anti-proliferative
VEGFR-2
Phosphorylated VEGFR-2, Caspase-3
Cell cycle arrest profile
Antimicrobial activity

ABSTRACT

A series of novel hybrid compounds of hexahydrobenzo[4,5]thieno[2,3-*d*]pyrimidine with aminothiazole scaffolds were synthesized. The synthesized compounds were evaluated for their cytotoxic activity against the NCI-60 human tumor cell line panel. Compounds **7c**, **7d** and **7e** exhibited significant antiproliferative activities at 10^{-5} M dose. Compound **7c** exhibited excellent cytotoxic activity against CNS cancer cell lines including SNB-75 and SF-295 as well as renal cancer cell line CAKI-1 when compared with sorafenib as standard anticancer drug. In addition, compound **7d** showed almost comparable anticancer activity to sorafenib against SNB-75 cell line and displayed moderate activity against SF-295 and CAKI-1 cell lines in comparison to sorafenib. Compound **7c** inhibited the vascular endothelial growth factor receptor 2 (VEGFR-2) with IC_{50} of 62.48 ± 3.7 nM and decreased both total VEGFR-2 and phosphorylated VEGFR-2 in treated SNB-75 cells suggesting its ability to down regulate cell proliferation, growth, and survival.. The flow cytometric analysis showed that **7c** displayed its cytotoxic activity through the reduction of the cellular proliferation and induction of cell cycle arrest at the G2/M phase. Compound **7c** clearly boosted the level of the apoptotic caspase-3. All the synthesized compounds were also screened for their antibacterial and antifungal activity against four pathogenic strains of both Gram-positive and Gram-negative as well as *Candida albicans*. Only compound **7d** exhibited antifungal activity against *Candida albicans* compared to nystatin as the standard antifungal compound.

1. Introduction

Anti-angiogenesis was suggested in 1971 by Folkman [1] as an important anticancer strategy based on the finding that tumor development was associated with increased vascularity [2]. The discovery of the VEGF pathway as a key regulator of angiogenesis led to the creation of a number of VEGF-targeted agents. VEGFs exert their biological effects through binding in an overlapping pattern to the kinase domain of three different, but structurally related VEGF receptors (VEGFRs 1–3). Upon binding to the extracellular domain of the receptors, they cause intracellular signaling in endothelial cells, resulting in proliferation and migration of these cells [3]. Therefore, angiogenesis suppression approaches based on the inhibition of VEGF/VEGFR signaling pathways are developing as attractive therapeutic methods for cancer management via inhibition of tumor angiogenesis and subsequent tumor growth progression [4]. VEGF has been validated as a therapeutic target in various types of human cancers including colorectal cancer [5], breast cancer [6], non-small cell lung cancer [7], renal cell cancer [8], glioblastoma multiforme [9]. VEGFR represent a family of three receptors including VEGFR-2, which is the key receptor for VEGF in the vascular endothelium, regulating different intracellular processes [10].

Sorafenib is a potent VEGFR-2 inhibitor and has been approved as a drug [11]. Most VEGFR-2 inhibitors shared four key pharmacophoric characteristics, according to a review of sorafenib and other VEGFR-2 inhibitors [12–15]. These features are shown in Fig. 1 and they include: (a) The main structure of most inhibitors comprises a flat aromatic or heteroaromatic ring structure, which occupies the catalytic ATP-binding domain and contributing in H-bond interaction with Cys919 residues located in the hinge area of the binding site. (b) A central aryl ring (hydrophobic spacer), occupying the linker region

* Corresponding author at: Pharmaceutical Organic Chemistry Department, Faculty of Pharmacy, Cairo University, Kasr El-Aini Street, Cairo 11562, Egypt (R.A. Hassan).

https://doi.org/10.1016/j.bioorg.2021.105137
Received 18 March 2021; Received in revised form 12 May 2021; Accepted 27 June 2021
Available online 1 July 2021

among the ATP binding domain and the DFG domain of the receptor. (c) A linker having a functional group acting as pharmacophore (e.g., amino or urea) that possesses both H-bond acceptor and donor to bind with two essential residues (Glu885 and Asp1046) in the DFG (Asp-Phe-Gly) motif, an essential tripeptide sequence in the active kinase domain. The NH motifs of the urea or amide moiety typically form one hydrogen bond with Glu885, while the C═O motif forms another hydrogen bond with Asp1046. (d) The terminal hydrophobic moiety of the inhibitors occupies the newly created allosteric hydrophobic pocket, revealed when the phenylalanine residue of the DFG loop flips out of its lipophilic pocket defining DFG-out or inactive conformation. In this allosteric binding region, hydrophobic interactions are typically accomplished [16]. Furthermore, analysis of the X-ray structure of various inhibitors bound to VEGFR-2 confirmed the required space available for different substituents around the terminal ring. [17].

Recently, thieno[2,3-*d*]pyrimidin-4-one derivatives, which are analogs of quinazoline alkaloids, have attracted the interest of medicinal chemistry researchers due to their wide range of biological and pharmaceutical activities [18]. Many thienopyrimidine based scaffolds have been developed and evaluated for their anticancer [19,20], antioxidant [21], antiinflammatory [22], antimicrobial [23], antiviral [24], antituberculosis [25], and anti-HIV activities [26]. Furthermore, numerous studies have been published on the synthesis of various quinazoline derivatives and their bioisosters; thienopyrimidines as potential anticancer agents acting through various mechanisms including the inhibition of cyclin dependent kinases (CDKs) [27], epidermal growth factor receptor (EGFR) [28], methionine synthase [29], *17β*-HSD1 [30], matrix metalloproteinases (MMPs) [31], P-glycoprotein (P-gp) modulation [32] (Fig. 2).

The tricyclic system, cycloalkylthieno[2,3-*d*]pyrimidine with different substitutions at position 4; has been used as a core for the mechanism-based design and synthesis of numerous anticancer agents targeting VEGFR-2 [33,34].

Thiazole nucleus is also an essential part of several clinically applied anticancer drugs, such as dasatinib, dabrafenib, ixabepilone, patellamide A, and epothilone [35]. Many thiazoles in conjugation with heterocyclic compounds have been studied for their VEGFR-2 kinase inhibitory activity as potential antitumor agents [35] (Fig. 3). These facts, in addition to the fact that amide linkages and thioethers are considered to contribute to the enhancement of the antitumor activity [36,37], influenced the design of our compounds in the current study.

Various cycloalkylthieno[2,3-*d*]pyrimidine derivatives combining these bioactive moieties were designed and evaluated for their anticancer activity. The goal of our research was to develop novel derivatives with the essential pharmacophoric features of the reported VEGFR-2 inhibitors with bioisosteric modifications at four different positions. A series of 4-chlorophenyl cycloalkylthieno[2,3-*d*] pyrimidines bearing various S-(substituted amino alkyl) moieties at position 2 rather than position 4, was synthesized. In this series, various thioether and amide containing linkers were used in the designed thienopyrimidne-aminothiazole hybrids to study the effect of these variations on the cytotoxic activity.

2. Results and discussion

2.1. Chemistry

Novel hexahydrobenzo[4,5]thieno[2,3-*d*]pyrimidine derivatives **7a-j** were synthesized according to Schemes 1 and 2. Substituted-2-aminothiazole derivatives **2a-e** were prepared by reaction of commercial aryl bromoethanones **1a-e** with thiourea according to a previously reported procedure [38]. 2-Chloro-*N*-(arylthiazol-2-yl)acetamide **3a-e** and 2-chloro-*N*-(arylthiazol-2-yl)propanamide derivatives **3f-j** were prepared through alkylation of substituted-aminothiazole derivatives **2a-e** with chloroacetyl chloride or 2-chloropropionyl chloride respectively in methylene chloride in presence of triethyl amine [38,39].

The initial intermediate ethyl 2-amino-4,5,6,7-tetrahydro[*b*]benzothiophene-3-carboxylate (**4**) was synthesized according to Gewald procedure [40]. Reacting compound **4** with 4-chlorophenyl isothiocyanate in absolute ethanol yielded ethyl 2-(3-(4-chlorophenyl) thioureido)-4,5,6,7-tetrahydrobenzo[*b*]thiophene-3-carboxylate (**5**) [41]. Treatment of compound **5** with potassium hydroxide in ethanol afforded the corresponding potassium 3-(4-chlorophenyl)-4-oxo-3,4,5,6,7,8-hexahydrobenzo[4,5]thieno[2,3-*d*]pyrimidine-2-thiolate **(6)** [41]. Reacting compound **6** with the key intermediates **3a-j** in absolute acetone in presence of anhydrous potassium carbonate afforded the target compounds hexahydrobenzo[4,5]thieno[2,3-*d*]pyrimidine derivatives **7a-j** in good to excellent yields.

All the newly synthesized compounds were characterized by ^{1}H NMR, ^{13}C NMR, IR and elemental analyses. ^{1}H NMR, ^{13}C NMR spectra are provided in the supplementary materials. IR spectra of derivatives **7a-j** revealed the presence of C═O stretching as a broad band in the range 1678–1693 cm^{-1}. The ^{1}H NMR of compounds **7a-j** were recorded in DMSO-d_6 for all the derivatives. ^{1}H NMR spectra of **7a-j** revealed the presence of aromatic proton of thiazole ring as a singlet signal in the range δ 7.63–7.97 ppm. Derivatives **7a-e** showed S-CH_2 protons as singlet signal at δ 4.18–4.19 ppm in ^{1}H NMR. While the ^{1}H NMR spectra of compounds **7f-j** showed a quartet at δ 4.71 ppm corresponding to S-CH-CH_3 and a doublet at δ 1.49–1.50 ppm corresponding to the methyl protons. ^{13}C NMR spectra of **7a-j** showed the presence of two carbonyl carbons in the range of δ 161.4–166.7 ppm and δ 166.7–170.7 ppm corresponding to the amidic linker and pyrimidone carbonyl groups respectively. Moreover, derivatives **7a-e** showed S-CH_2 carbon at δ 36.3 ppm. While, S-CH-CH_3 of compounds **7f-j** appeared as two signals at the

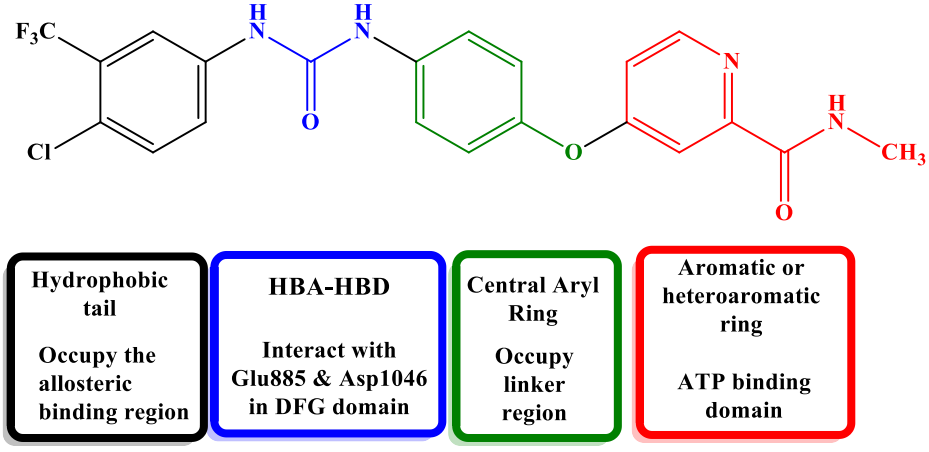

Fig. 1. The basic structural requirements for sorafenib as reported VEGFR-2 inhibitor.

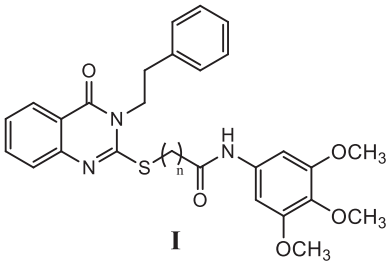

I

n=1,2 GI_{50} = 2.02 µM
EGFR inhibitor (colon cancer)

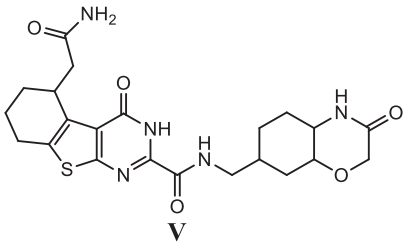

V

IC_{50}= 7.4 nM
MMP-8 inhibitor

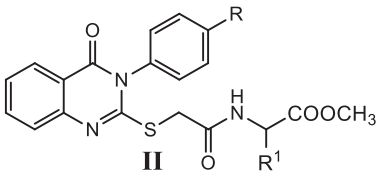

II

R= H, CH_3, OCH_3.
R^1= H, CH_2OH
IC_{50}=20.6-34 µg/mL (prostate cancer)
Methionine Synthase inhibitors

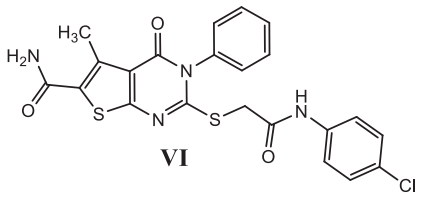

VI

GI%= 116.09 (melanoma),
79.38 (ovarian cancer),
47.22 (Renal cancer)

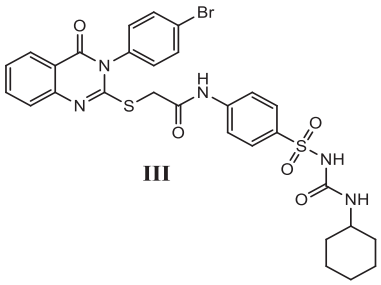

III

IC_{50}= 7.8 µM (HepG)
IC_{50}=5.3 µM (VEGFR-2)
VEGFR-2 inhibitors

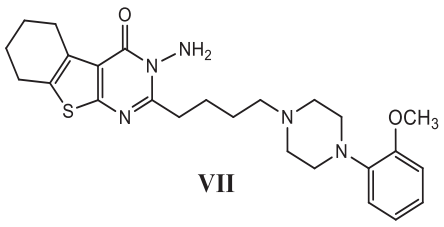

VII

IC_{50}= 2.01 µg/ml (HCT-116),
1.07 µg/ml (HELA)
1.61 µg/ml (HEP2)

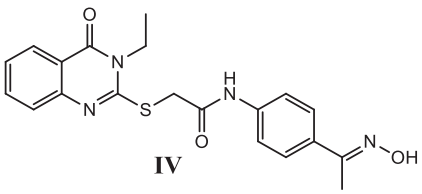

IV

IC_{50}= 3.97 µM (Hep G)
IC_{50}=2.5 µM (VEGFR-2)
VEGFR-2 inhibitors

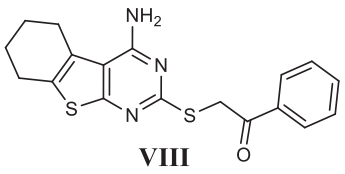

VIII

EC_{50}=0.64 µM
P-glycoprotein modulator

Fig. 2. Structures of some reported quinazoline derivatives and thieno[2,3-*d*]pyrimidne derivatives with cytotoxic activity.

range δ 17.3–17.6 ppm for CH_3 and at the range δ 45.8–45.9 ppm for S-CH carbon.

2.2. Biological evaluation

2.2.1. Anticancer activity

2.2.1.1. In vitro cytotoxic activity against a panel of 60 human tumor cell lines. In this study, all the newly synthesized compounds were selected by National Cancer Institute (USA) [42] for anticancer evaluation under the Developmental Therapeutic Program (DTP) [43–46]. The selected compounds were evaluated at one dose (10^{-5} M) against 60 different human tumor cell lines, representing leukemia, melanoma and tumor of lung, colon, central nervous system (CNS), ovary, kidney, prostate and breast. The growth inhibition percentages obtained from the single dose test are shown in Table 1. In light of the NCI screening results, the following observations could be outlined. Compounds **7c** and **7d** exhibited the most potent anticancer activity against CNS cancer cell lines SF-295, SNB-75 and renal cell line CAKI-1 with growth inhibition percentages 57.59, 58.35 and 50.99 respectively for **7c** and 45.35, 46.94 and 52.39 respectively for **7d**. In addition, compounds **7c** and **7d** exhibited moderate anticancer activity against CNS cancer cell line SF-268 with cell growth inhibition of 30.38% and 29.7% respectively. Compound **7e** showed moderate anticancer activity against CNS cancer cell line SF-295 with cell growth inhibition 35.87%. Compounds **7c** and **7d** exhibited moderate anticancer activity against four non-small cell lung cancer cell lines, including A549/ATCC, NCI-H226, NCI-H23 and NCI-H522 with cell growth inhibition 29.63%, 36.03%, 43.13% and

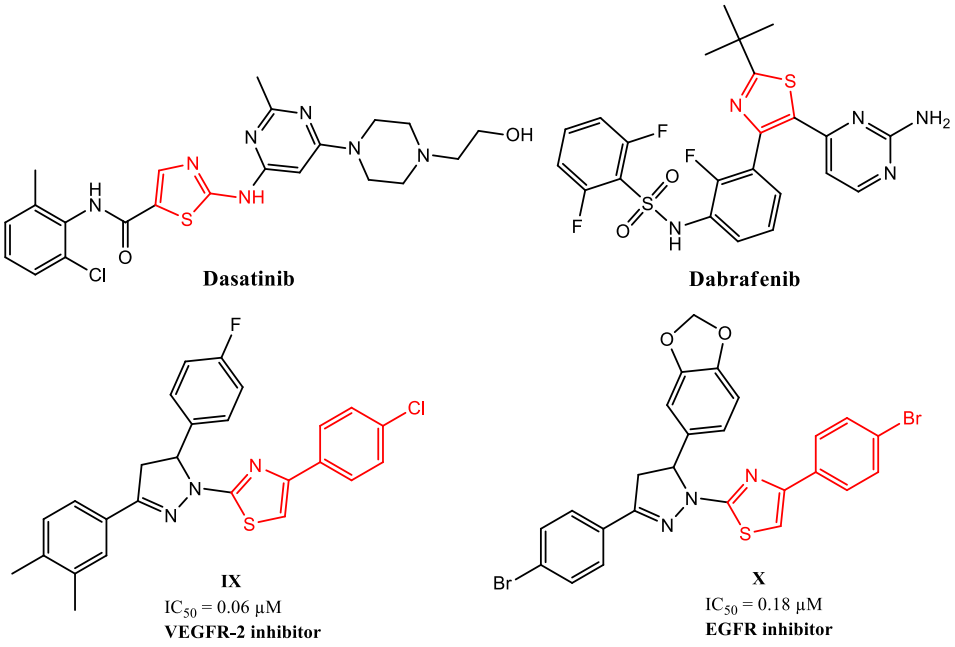

Fig. 3. Thiazole containing anticancer drugs and some thiazole derivatives, as VEGFR/EGFR inhibitors.

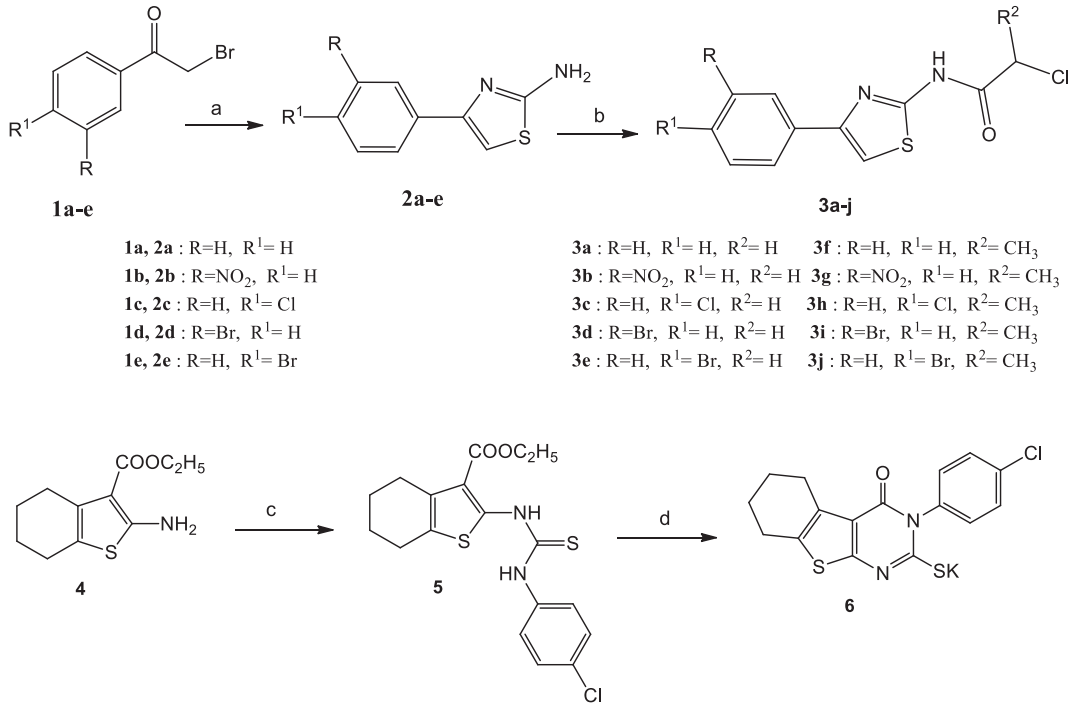

Scheme 1. Synthesis of aryl thiazole derivatives **3a-j** and intermediates **4,5 and 6 Reagents and conditions**: a) Thiourea ethanol anhydrous Na aetate, R.T, 4h; b) Chloroacyel chloride or 2-chloropropionylchloride CH_2Cl_2, TEA R.T 4h; c) 4-Chlorophenyl isothicyanate, ethnol reflux 9h; d) KOH ehanol reflux 6h.

30.21% respectively for **7c** and 42.47%, 28.25%, 37.6% and 31.51% respectively for **7d**. Compound **7c** exhibited also moderate anticancer activity against one colon cancer cell line HT29 with growth inhibition 38.34%. Likewise, compound **7f** demonstrated moderate anticancer activity against colon cancer cell line HCT-15 with growth inhibition 43.9%. Compound **7d** showed moderate anticancer activity against two colon cancer cell lines HCT-116 and HT29 with cell growth inhibition 39.28% and 32.98% respectively. Compound **7c** displayed moderate anticancer activity against one ovarian cancer cell line OVCAR-8 with growth inhibition percentage 31.86 and lower inhibitory activity against ovarian cell lines IGROV1 and OVCAR-4 with cell growth inhibition 27.37% and 27.14% respectively, while compound **7d** showed moderate anticancer activity against two ovarian cancer cell lines IGROV1 and OVCAR-8 with cell growth inhibition 29.76% and 32.89% respectively. Compound **7c** was effective moderately against two prostate cancer cell lines including PC-3 and DU-145 with growth inhibition percentage 42.45 and 31.45 respectively, while compound **7d** showed moderate anticancer activity against prostate cancer cell line PC-3 with cell growth inhibition 41.63% and lower inhibition against prostate cancer cell line DU-145 with cell growth inhibition 25.48%. Only

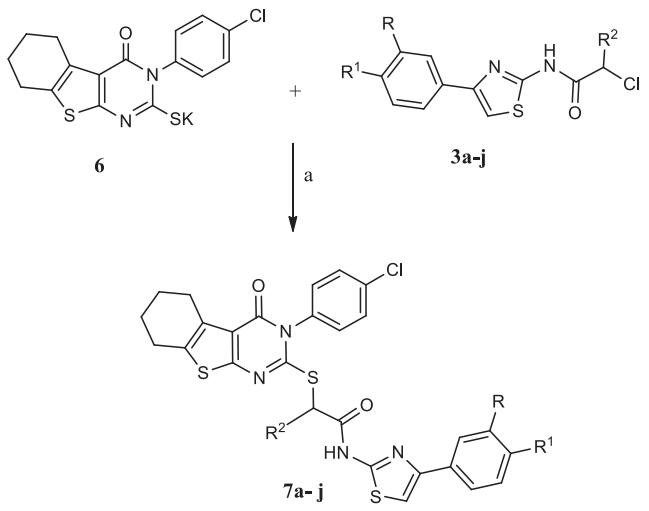

7a : R=H, R^1= H, R^2= H **7f** : R=H, R^1= H, R^2= CH_3
7b : R=NO_2, R^1= H, R^2= H **7g** : R=NO_2, R^1= H, R^2= CH_3
7c : R=H, R^1= Cl, R^2= H **7h** : R=H, R^1= Cl, R^2= CH_3
7d : R=Br, R^1= H, R^2= H **7i** : R=Br, R^1= H, R^2= CH_3
7e : R=H, R^1= Br, R^2= H **7j** : R=H, R^1= Br, R^2= CH_3

Scheme 2. Sysnhesis of the target compounds hexahydrobenzo[4,5]thieno[2 3-*d*]pyrimidine **7a-j** Reagents and conditions a) Absolute aceone, reflux 15-20h.

compound **7c** displayed moderate anticancer activity against breast cancer cell line MDA-MB-468 and HS 578T with cell growth inhibition 34.92% and 27.44% respectively. Finally, it is worth mentioning, that all the tested compounds showed inhibition activity against renal cancer cell line UO-31 with cell growth inhibition between (14.97–25.89%). Compounds **7a,b** and **7 g-j** showed no activity against most investigated cancer cell lines.

2.2.1.2. In vitro antiproliferative activity. Antiproliferative activity of compounds **7c** and **7d** was examined against three human tumor cell lines, namely, CNS cancer; SF-295 and SNB-75 and renal cancer; CAKI-1. Activity of compound **7e** was only examined against CNS cancer SF-295 in light of its growth inhibition percentages obtained from the single dose screening. MTT (3-(4,5-dimethylthiazol-2-yl)-2,5 diphenyl tetrazolium bromide) colorimetric assay protocol was used as described by Mosmann [47]. Sorafenib and doxorubicin were included in the experiments as reference cytotoxic drugs. The results were expressed as growth inhibitory concentration (IC_{50}) values, which represent the compound's concentration required to produce 50% inhibition of cell growth after 72hr of incubation. IC_{50} values were calculated from the concentration–inhibition response curve and summarized in Fig. 4**.** Investigations of the cytotoxic activity showed that compound **7c** was the most potent derivative against SNB-75, SF-295 and CAKI-1 cell lines with IC_{50} = 7.12 ± 0.33, 7.36 ± 0.39 and 4.84 ± 0.22 μM respectively as compared to the IC_{50} of sorafenib of 14.77 ± 0.68, 14.3 ± 0.76 and 7.23 ± 0.33 μM respectively. Compound **7d** showed almost equipotent anticancer activity (IC_{50} = 16.36 ± 0.76 μM) to sorafenib against SNB-75 cell line. Compound **7d** also displayed moderate activity (IC_{50} = 20.1 ± 1.08 μM) against SF-295 cancer cell line in comparison to sorafenib and weak activity (IC_{50} = 22.52 ± 1.04 μM) against CAKI-1 renal cancer cell line in comparison to sorafenib. Compound **7e** displayed almost equipotent activity (IC_{50} = 17.7 ± 0.94 μM) compared to sorafenib (IC_{50} = 14.3 ± 0.76 μM) against SF-295 cell line. All tested compounds showed weak activity compared to doxorubicin against SNB-75, SF-295 and CAKI-1 cell lines with exception to compound **7c** which showed 0.75-fold the activity of doxorubicin against SF-295 CNS cell line.

2.2.1.3. Measurement of the inhibitory activity on VEGFR-2. Thienopyrimidine and aminothiazole scaffolds are parts of numerous potent VEGFR-2 kinase inhibitors. Therefore, to confirm the VEGFR-2 kinase binding site as a possible target of action to the synthesized derivatives, the most active antiproliferative derivatives **7c**, **7d** and **7e** were selected to evaluate their inhibitory activity against VEGFR-2 using the VEGFR-2 kinase inhibitory kit assay. The results were reported as a 50% inhibition concentration value (IC_{50}) calculated from the concentration–inhibition response curve and summarized in Fig. 5. Doxorubicin and sorafenib were used as positive controls in this assay. The tested compounds **7c** and **7e** showed better inhibitory activity than doxorubicin (IC_{50} = 86.01 ± 5.0 nM) with IC_{50} values 62.48 ± 3.7 and 79.71 ± 4.7 nM respectively. Meanwhile, compound **7d** showed the least inhibitory activity with IC_{50} value 128.1 ± 7.5 nM. All tested compounds **7c**, **7d** and **7e** displayed less inhibitory activity compared to sorafenib.

2.2.1.4. Measurement of the effect of compound 7c on the total concentration of VEGFR-2. The total concentration of VEGFR-2 was evaluated in SNB-75 CNS cancer cell line using the IC_{50} of compound **7c** (7.12 μM) to assess its ability to down-regulate this key receptor. The results indicate that compound **7c** can down-regulate VEGFR-2 by 78.5% compared to the untreated SNB-75 as shown in Fig. 6. These results suggest that **7c** has a down-regulating effect on VEGFR-2 expression.

2.2.1.5. Measurement of the effect of compound 7c on the phosphorylation of VEGFR-2. The ability of compound **7c** to directly inhibit VEGFR-2 phosphorylation (the active form of VEGFR-2) at its IC_{50} concentration (7.12 μM) was evaluated in SNB-75 cells using an *in vitro* kinase assay with VEGFR-2 (Phospho-Tyr951) Colorimetric Cell-Based ELISA Kit. The results showed that compound **7c** can interfere with VEGFR-2 phosphorylation by 58.44% compared to the untreated SNB-75 cells (Fig. 7). All the previous findings suggest that the thienopyrimidine derivative **7c** will lower both total VEGFR-2 and phosphorylated VEGFR-2 in treated SNB-75 cells compared to untreated SNB-75 cells suggesting that **7c** has down-regulating effect on cell proliferation, growth, and survival.

2.2.1.6. Molecular docking in the active site of VEGFR-2. In order to study the binding features of the newly synthesized compounds in the binding site of VEGFR-2, the molecular modeling studies were carried out using Molecular Operating Environment (MOE, 2019.0102) software. All minimizations were performed with MOE until an RMSD gradient of 0.05 kcal•$mol^{-1}Å^{-1}$ with MMFF94x force field and the partial charges were automatically calculated. The X-ray crystallographic structure of VEGFR-2 co-crystalized with sorafenib (PDB ID: 4ASD) was downloaded from the protein data bank (https://www.rcsb.org/structure/4ASD). Through examination of the binding interactions of sorafenib to the active site of the receptor, it shows H-bond interactions with the key amino acids Glu885, Cys919, Cys1045 and Asp1046 (Fig. 8**A**).

Docking setup was first validated by self-docking of the co-crystallized ligand (sorafenib) in the vicinity of the binding site of the receptor, the docking score (S) was −10.2499 kcal/mol. and root mean square deviation (RMSD) was 0.1511 Å (Fig. 8**B and 8C**).

The validated setup was then used in predicting the ligand-receptor interactions at the binding site for compounds **7c**, **7d** and **7e**. The ability of the target compounds to interact with the key amino acids in the binding site rationalizes their good activity as indicated by their docking pattern and docking scores compared to that of sorafenib. The three tested compounds showed good binding scores ranging from −9.8363 kcal/mol. to −8.7776 kcal/mol. and they exhibited similar fit to sorafenib into the binding pocket of the target receptor with similar binding interactions. The results are summarized in Table 2 and Figs. 9, 10 and 11**.**

Table 1
Growth inhibition percentages obtained from the single dose (10^{-5} M) test of compounds **7a-j**.

Panel/ cell line	Compound									
	7a	**7b**	**7c**	**7d**	**7e**	**7f**	**7 g**	**7 h**	**7i**	**7j**
Leukemia										
CCRF-CEM	–	–	12.25	16.39	–	–	–	–	–	–
HL-60(TB)	–	–	–	–	–	–	–	–	–	–
K-562	–	–	–	–	–	–	–	–	–	–
MOLT-4	–	–	12.95	–	–	–	–	–	–	–
RPMI-8226	13.33	–	–	–	–	–	–	–	–	–
SR	–	–	19.42	18.19	–	15.07	–	–	–	–
Non-Small Cell Lung Cancer										
A549/ATCC	–	–	29.63	42.47	–	–	–	–	–	–
EKVX	–	–	25.02	19.80	14.09	15.32	15.7	11.8	17.47	–
HOP-62	–	–	–	–	–	–	–	–	–	–
HOP-92	–	–	–	–	–	–	–	–	–	–
NCI-H226	–	–	36.03	28.25	14.43	–	–	–	–	–
NCI-H23	–	–	43.13	37.6	–	–	12.2	–	–	–
NCI-H322M	–	–	12.18	17.7	–	–	14.19	–	–	–
NCI-H460	–	–	–	–	–	–	–	–	–	–
NCI-H522	–	14.11	30.21	31.51	15.03	18.15	13.44	–	14.76	17.94
Colon Cancer										
COLO 205	–	–	14.86	–	–	–	–	–	–	–
HCC-2998	–	–	–	–	–	–	–	–	–	–
HCT-116	–	–	18.4	39.28	–	10.00	–	–	–	–
HCT-15	–	–	12.23	12.25	–	43.9	–	–	–	–
HT29	–	–	38.34	32.98	11.98	–	–	–	–	–
KM12	–	–	16.17	15.17	–	–	–	–	–	–
SW-620	–	–	21.15	24.77	–	–	–	–	–	–
CNS Cancer										
SF-268	–	–	30.38	29.7	–	12.51	11.55	–	–	–
SF-295	23.37	–	57.59	45.35	35.87	16.22	–	–	–	–
SF-593	–	–	–	–	–	–	–	–	–	–
SNB-19	–	–	15.24	13.18	–	–	–	–	–	–
SNB-75	–	12.04	58.35	46. 94	11.69	14.84	–	–	14.74	–
U251	–	–	21.24	21.91	–	10.32	–	–	–	–
Melanoma										
LOX IMVI	–	–	15.72	26.63	–	–	–	–	–	–
MALME-3M	–	–	–	10.29	–	–	–	–	–	–
M14	–	–	23.44	–	–	–	–	–	–	–
MDA-MB-435	–	–	–	–	–	–	–	–	–	–
SK-MEL-2	–	–	–	–	–	–	–	–	–	–
SK-MEL-28	–	–	15.59	–	–	–	–	–	–	–
SK-MEL-5	–	–	17.18	14.11	–	–	–	–	–	–
UACC-257	–	–	–	–	–	–	–	–	–	–
UACC-62	12.05	–	14.92	19.13	19.04	–	–	13.68	–	11.05
Ovarian Cancer										
IGROV1	–	12.34	27.37	29.76	15.07	–	–	–	13.97	–
OVCAR-3	–	–	10.96	14.32	–	–	–	–	–	–
OVCAR-4	–	–	27.14	12.89	–	–	–	–	–	–
OVCAR-5	–	–	24.35	–	10.59	–	–	–	13.46	–
OVCAR-8	–	–	31.86	32.89	–	–	–	–	–	–
NCI/ADR-RES	–	–	19.52	24.23	–	–	–	–	–	–
SK-OV-3	–	–	–	–	–	–	–	–	–	–
Renal Cancer										
786-0	–	–	–	–	–	–	–	–	–	–
ACHN	–	–	–	12.97	–	–	–	–	–	–
CAKI-1	11.16	–	50.99	52.39	15.17	10.07	10.83	–	–	–
RXF 393	–	–	–	–	–	–	–	–	–	–
SN12C	–	–	20.46	11.55	–	–	–	–	–	–
TK-10	–	–	–	–	–	–	–	–	12.51	–
UO-31	17.93	14.79	25.36	25.35	25.89	20.25	24.47	15.95	23.36	18.54
Prostate Cancer										
PC-3	–	–	42.45	41.63	–	10.4	–	–	–	–
DU-145	–	–	31.45	25.48	–	–	–	–	–	–
Breast Cancer										
MCF7	–	–	12.65	17.76	15.23	17.37	10.39	10.09	–	–
MDA-MB-231/ATCC	–	–	19.28	19.65	–	–	–	–	–	10.94
HS 578T	–	–	27.44	10.05	–	–	–	–	–	–
BT-549	–	–	–	–	–	–	–	–	–	–
T-47D	–	–	23.07	23.81	–	–	–	–	–	–
MDA-MB-468	–	–	34.92	–	10.55	12.27	–	–	–	–
Mean Inhibition*	0	0	18.30	16.83	4.35	5.14	3.57	1.66	2.62	1.87

– Growth inhibition percentage produced by the compound is lower than 10%.
* Mean inhibition was calculated according to GI% values over all NCI- 60 cell lines

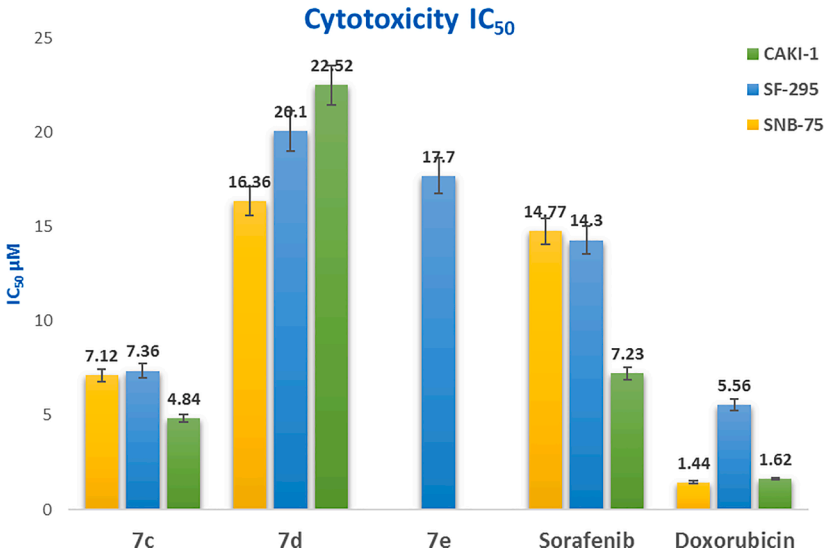

Fig. 4. Graphical representation for concentrations required for 50% inhibition of cell viability (IC_{50}) of compounds **7c**, **7d** and **7e** compared to doxorubicin and sorafenib.

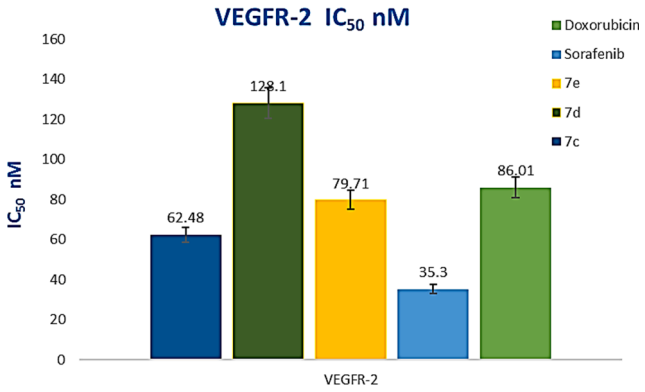

Fig. 5. Graphical representation for concentrations required for 50% inhibition of VEGFR-2 (IC_{50}) of compounds **7c**, **7d** and **7e** compared to doxorubicin and sorafenib.

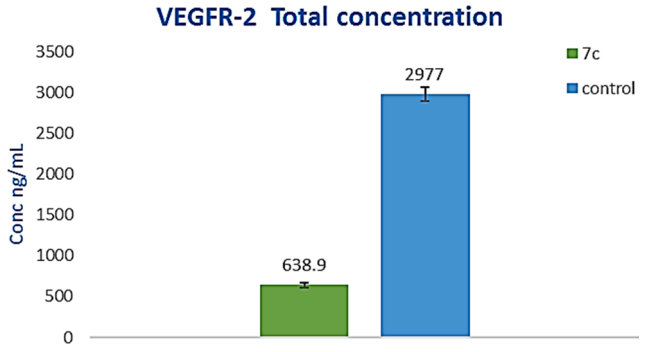

Fig. 6. Graphical representation to show that **7c** treated SNB-75 cells showed decrease in the total concentration of VEGFR-2 compared to the control untreated cells.

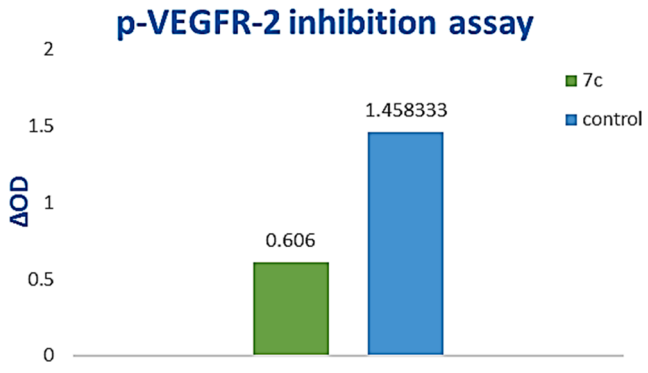

Fig. 7. Graphical representation to show that **7c** treated SNB-75 cells will lower the phosphorylated VEGFR-2 compared to control untreated cells.

2.2.1.7. Structure activity relationship. Structure Activity Relationship studies were performed for the two synthesized series of thienopyrimidine–aminothiazole hybrids **7a-e** and **7f-j**. In the first series the percentage of inhibition pattern for the compounds in Table 1 showed that substitution with weak electron withdrawing halogen atom (4-chlorophenyl **7c**, 3-bromophenyl **7d** or 4-bromophenyl **7e**) yields more potent cytotoxic agents. Particularly the 4-chloro derivative **7c** which exhibited the highest mean of inhibition percentage over the 60 cell line panel equal to 18.32% (Table 1). The unsubstituted phenyl derivative **7a** and the derivative substituted with strong electron withdrawing 3-nitro group **7b** showed low cytotoxic activity along all tested cell lines.

Confirming the importance of the 4-chloro substitution; compound **7c** displayed the highest inhibition percentage against SNB-75, SF-295 and CAKI-1 cell lines in the single dose *in vitro* cytotoxic screening (Table 1). Moreover, compound **7c** showed sensitivity against higher number of tested cell lines among halogen substituted derivatives (**7c-7e**). Investigations of the *in vitro* anti proliferative assay indicated that compound **7c** was the most potent derivative against SNB-75, SF-295 and CAKI-1 cell lines in comparison to sorefinib as reference drug (Fig. 4). In addition, the favorable interactions displayed by compound **7c** with the key amino acids at the VEGFR-2 active site was comparable

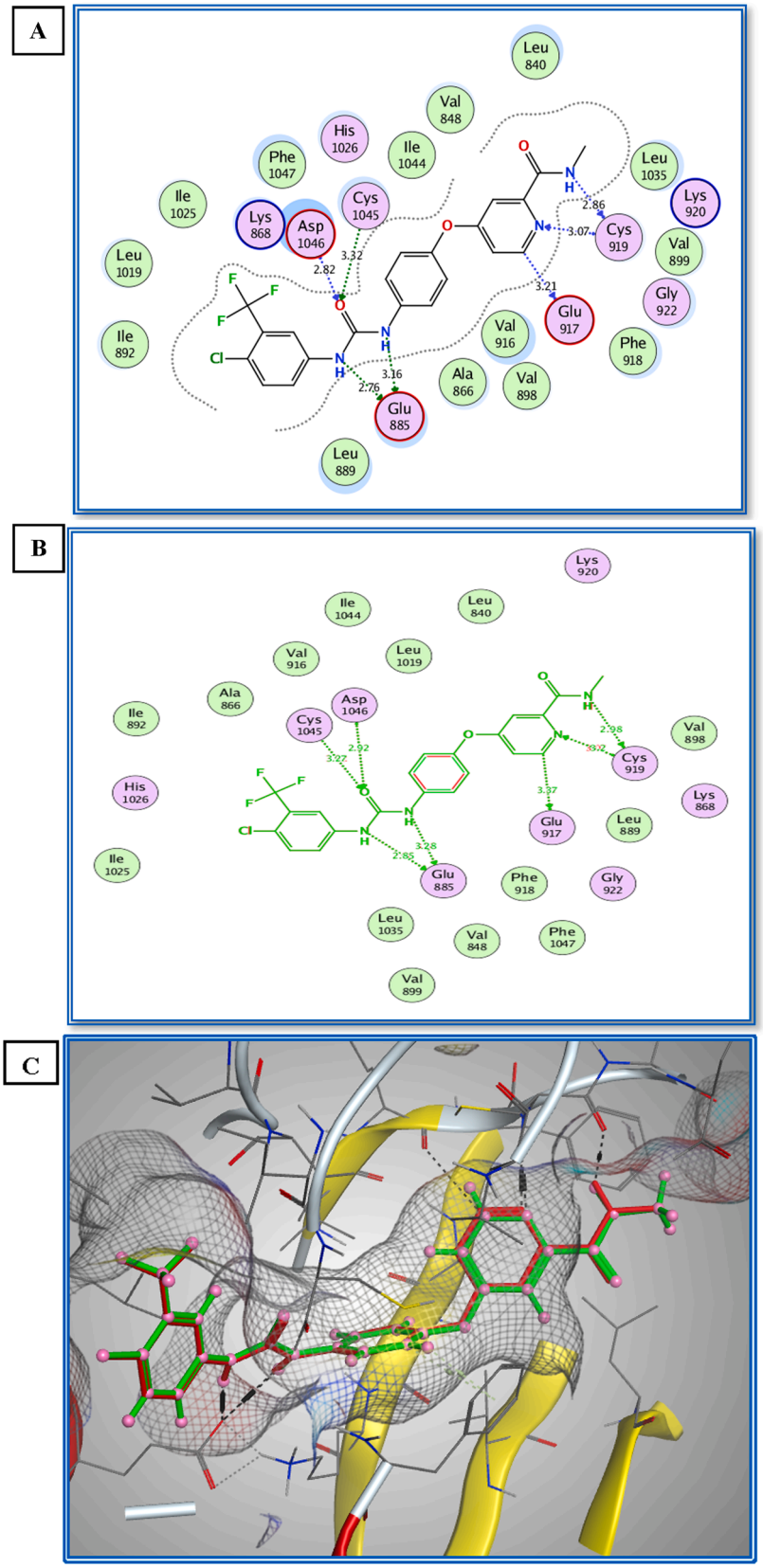

Fig. 8. A) 2D interactions of sorafenib within VEGFR-2 active site; **B)** and **C)** 2D representation and 3D representation of the superimposition of the co-crystallized (red) and the docking pose (green) of sorafenib in the active site of VEGFR-2. (For interpretation of the references to color in this figure legend, the reader is referred to the web version of this article.)

Table 2
Docking scores, hydrogen bonds and interactions of tested compounds and sorafenib inside VEGFR-2 binding site (PDB entry 4ASD).

Compound	S (kcal/mol)	Amino acids	Interacting groups	Type of interaction	Length
Sorafenib	−10.2499	Glu885	NH (urea)	H-bond donor	2.76
		Glu885	NH (urea)	H-bond donor	3.16
		Cys919	NH (amide)	H-bond donor	2.86
		Cys919	N (pyridine)	H-bond	3.07
		Cys1045	O (C═O)	acceptor	3.32
		Asp1046	O (C═O)	H-bond acceptor	2.82
				H-bond acceptor	
7c	−9.0323	Glu855	S (thiazole)	Non-classical	4.40
		Glu885	S	(σ hole)	4.05
		Leu889	(thiophene)	H-bond	3.87
		Cys919	S	acceptor	4.03
		Cys1045	Cl	H-bond	3.67
		Asp1046	N (thiazole)	acceptor	2.92
			NH	Electrostatic	
				H-bond acceptor	
				H-bond donor	
7d	−8.7776	Glu885	S	Non-classical	3.82
		Val899	(thiophene)	(σ hole)	4.05
		Cys919	N (thiazole)	H-bond	3.52
		Leu1053	Br	acceptor	4.04
		Ile1044	N (thiazole)	Halogen bond	3.75
		Asp1046	Cl	H-bond	3.25
			CH_2	acceptor	
				Electrostatic	
				H-bond donor	
7e	−9.8363	Glu885	NH	H-bond donor	3.53
		Val899	N (thiazole)	H-bond	3.96
		Val914	S (thiazole)	acceptor	4.23
		Cys1045	O (C═O)	Non-classical	3.13
		Asp1046	O (C═O)	(σ hole)	2.95
		Asp1046	CH_2	H-bond acceptor	3.99
				H-bond acceptor	
				Electrostatic	

to that of sorefinib (Fig. 9) which may explain its remarkable VEGFR-2 inhibitory activity.

Replacing the chlorine atom in compound **7c** with bromine atom in compound **7e** at para position leads to decline in the activity. Compound **7e** exhibited mean of inhibition equals 4.35%. Also, inhibition percentages among SNB-75, SF-295 and CAKI-1 cell lines were reduced, in addition to reduction in number of affected cell lines in comparison to compound **7c**. The decline in activity was also observed in the *in vitro* anti proliferative assay against SF-295 cell line with $IC_{50} = 17.7 \pm 0.94$ μM compared to **7c** with $IC_{50} = 7.36 \pm 0.39$ μM against the same tested cell line (Fig. 4).

Furthermore, switching the position of the bromo group from para in **7e** to meta position in **7d** led to increase in the mean of inhibition from 4.35% for **7e** to 16.83% for **7d** (Table 1), indicating the important cytotoxic effect of the meta position of bromo group in **7d**. Besides, it is noticeable that compound **7d** was nearly as active as the most potent cytotoxic derivative **7c** against most cell lines in the single dose *in vitro* cytotoxic screening. On the other hand, 3-bromophenyl derivative **7d** showed decrease in activity against SNB-75, SF-295 and CAKI-1 cell lines in comparison to 4-chlorophenyl derivative **7c** upon conducting *in vitro* anti proliferative assay.

Substitution of R^2 with a methyl group in the thienopyrimidine derivatives led to synthesis of the second series **7f-j.** Comparing *in vitro* cytotoxic activity with the first series revealed that halogen substituted derivatives including 4-chlorophenyl **7 h**, 3-bromophenyl **7i** or 4-bromophenyl **7j**, showed marked decrease in inhibitory activity with most cell lines and marked decrease in the mean of inhibition percentages than the halogenated derivatives **7c-e**. On the other hand, the unsubstituted phenyl derivative **7f** and 3-nitrophenyl derivative **7 g** showed an increase in the mean of inhibition percentages compared to compounds **7a** and **7b**.

2.2.1.8. Cell cycle analysis. Anticancer mediators exert their cytotoxic action by terminating cellular proliferation at definite checkpoints which are distinct stages in the cell cycle. Suppression of these phases results in termination of the cell proliferation. Cell cycle analysis employs flow cytometry to discriminate cells within the different cell cycle phases. In this work, the most active compound in cytotoxic assay **7c** was further exposed to cell cycle analysis to explore the definite phase at which cell cycle arrest takes place in the SNB-75 CNS cancer cell line. SNB-75 cells were exposed to compound **7c** at its IC_{50} (7.12 μM) for 24 h and its effect on the cell population in different cell phases was recorded and presented in Fig. 12. Exposure of SNB-75 cells to compound **7c** resulted in significant drop in the cell population at the G0-G1 and S phases with 14.26% and 21.68%, respectively. Moreover, marked increase in the proportion of cells in the G2/M phase by 2.5-fold, and in the pre-G1 phase by 23.8-fold, in comparison to the control (DMSO) was observed. This evidently shows that the target thienopyrimidine derivative **7c** stopped the cell cycle proliferation of SNB-75 cells in the G2/M phase.

2.2.1.9. Apoptosis determination by Annexin V-FITC assay. Annexin V-based flow cytometry test represents a helpful approach for eterming whether death of cells is attributed to programmed apoptosis or to uncontrolled necrosis. To ensure the ability of compound **7c** to induce apoptosis, a cytofluorimetric analysis was performed using propidium iodide (PI), which stains DNA and enters only dead cells, and fluorescent immunolabeling of the Annexin-V protein. Annexin-V binds to phosphatidylserine (PS) expressed only on the surface of the apoptotic cells and fluoresces green after interacting with the fluorochrome labeled Annnexin-V. On the other hand, PI stains DNA and enters only dead cells [48]. Dual staining for Annexin-V and PI permits discrimination between live cells, early apoptotic cells, late apoptotic cells and necrotic cells. Compound **7c** was selected to be tested for its effect on the cell cycle of the SNB-75 cell line since it showed the highest anticancer action toward this cell line. As shown in Fig. 13, after 24 h of treatment of SNB-75 cells with compound **7c** at its IC_{50} concentration (7.12 μM), a decrease in the percentage of the survived cells was observed. The results revealed an elevation in the apoptotic cells percentage in early apoptosis phase from 0.27% to 4.71% and a significant elevation in late apoptosis phase from 0.07% to 21.3%. In late stage of apoptosis, caspase and independent routes are mediated leading to DNA fragmentation, and nuclear condensation. Furthermore, an elevation in the cells percentage in necrosis phase from 1.39% to 15.26% was observed. This corresponds to an increase in the total apoptosis percentage from 1.73% to 41.27%.

2.2.1.10. The effect of compound 7c on the apoptotic marker level (Caspase-3). The stimulation of caspases as caspase-3 is responsible for apoptosis. Caspase-3 is an effector caspase that has a vital role in apoptosis. It is activated through one of the initiator caspases which leads to activation of certain enzymes responsible for fragmentation of DNA [49]. Therefore, the apoptosis induction by compound **7c** in SNB-75 cells was examined via a caspase-3 assay, compared to doxorubicin and sorafenib as reference drugs. Compound **7c** clearly boosted the level of the apoptotic caspase-3 by 9.29-fold compared to sorafenib which increased the level of caspase-3 by 8.16-fold (Fig. 14). On the other hand, doxorubicin increased the level of caspase-3 by 12.8-fold. This proposed that compound **7c** might prompt apoptosis via a caspase-dependent mechanism.

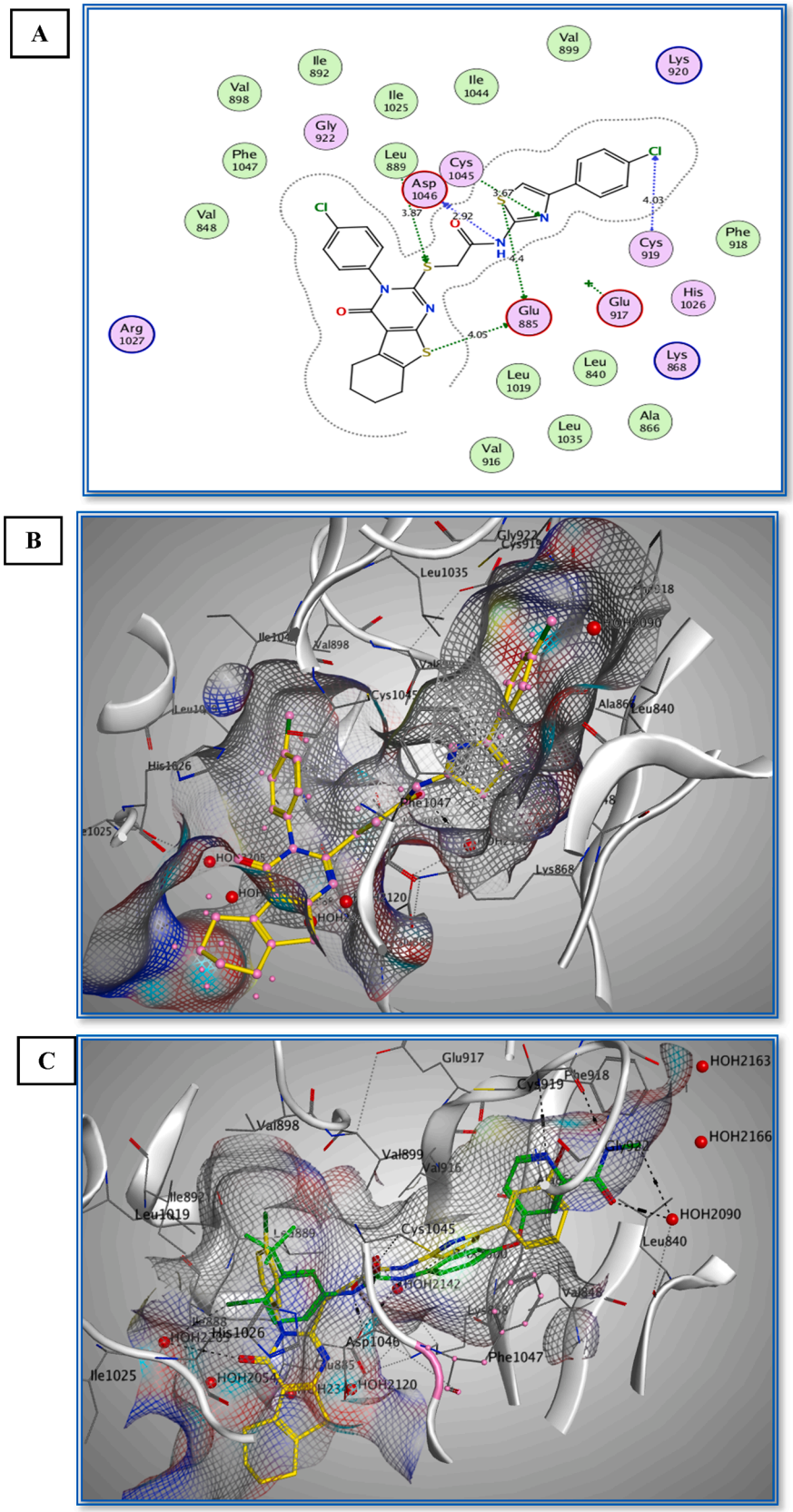

Fig. 9. A) 2D interactions of compound **7c** within VEGFR-2 active site**; B)** 3D diagram of compound **7c** interactions within VEGFR-2 binding site; **C)** 3D diagram of compound **7c** superimposed with sorafenib interactions within VEGFR-2 binding site.

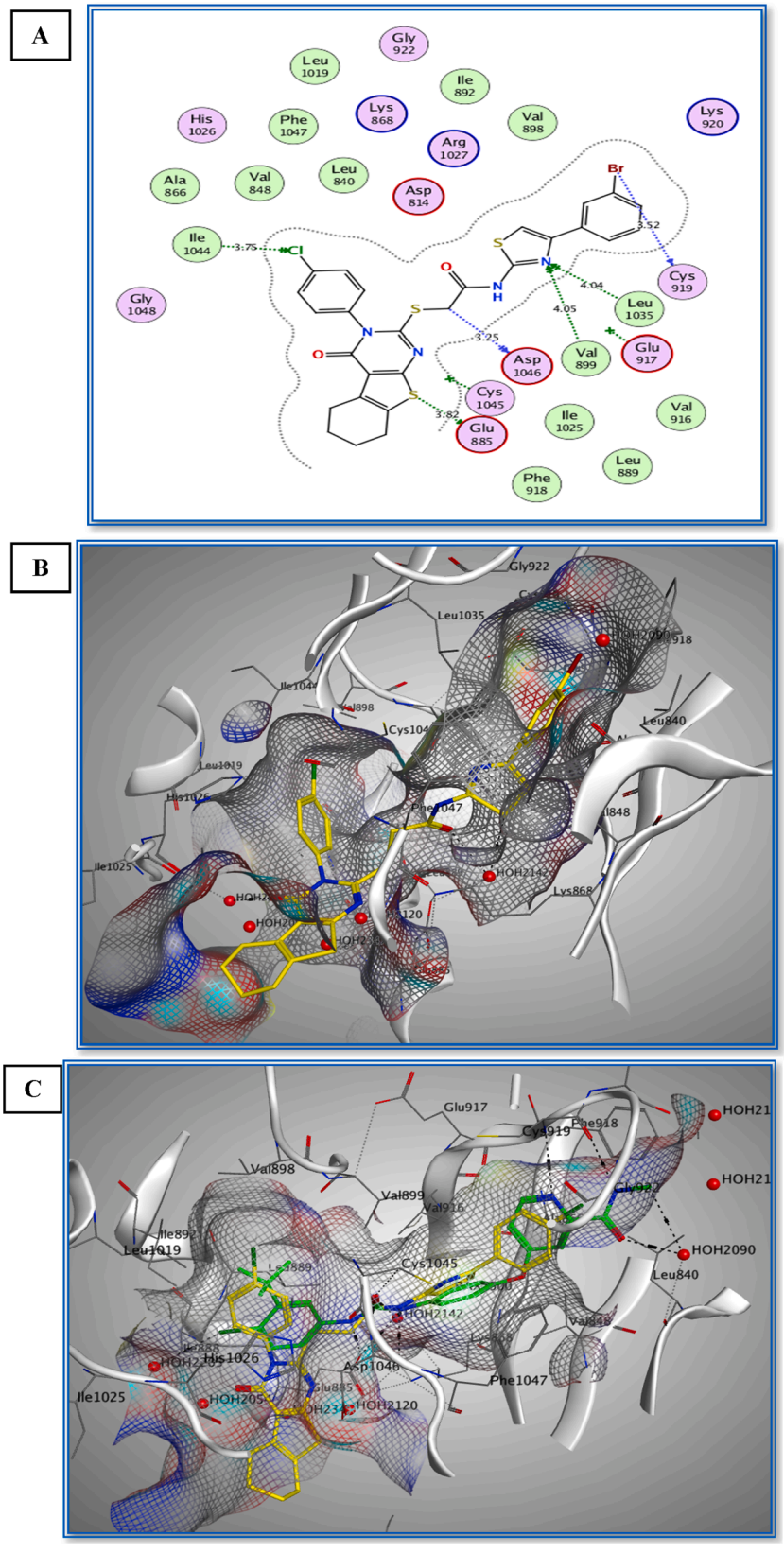

Fig. 10. A) 2D interactions of compound **7d** within VEGFR-2 active site; **B)** 3D diagram of compound **7d** interactions within VEGFR-2 binding site; **C)** 3D diagram of compound **7d** superimposed with sorafenib interactions within VEGFR-2 binding site.

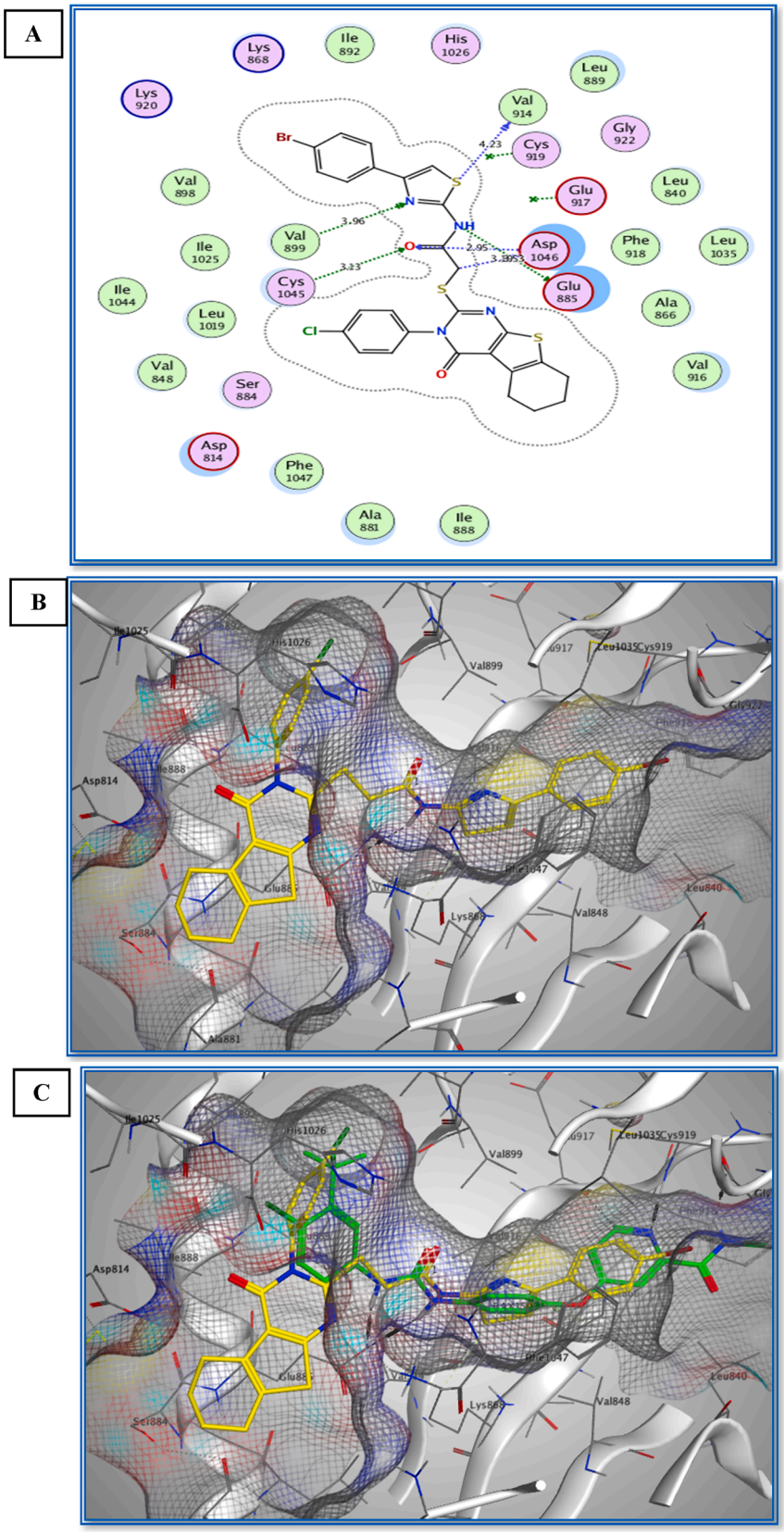

Fig. 11. A) 2D interactions of compound **7e** within VEGFR-2 active site; **B)** 3D diagram of compound **7e** interactions within VEGFR-2 binding site; **C)** 3D diagram of compound **7e** superimposed with sorafenib interactions within VEGFR-2 binding site.

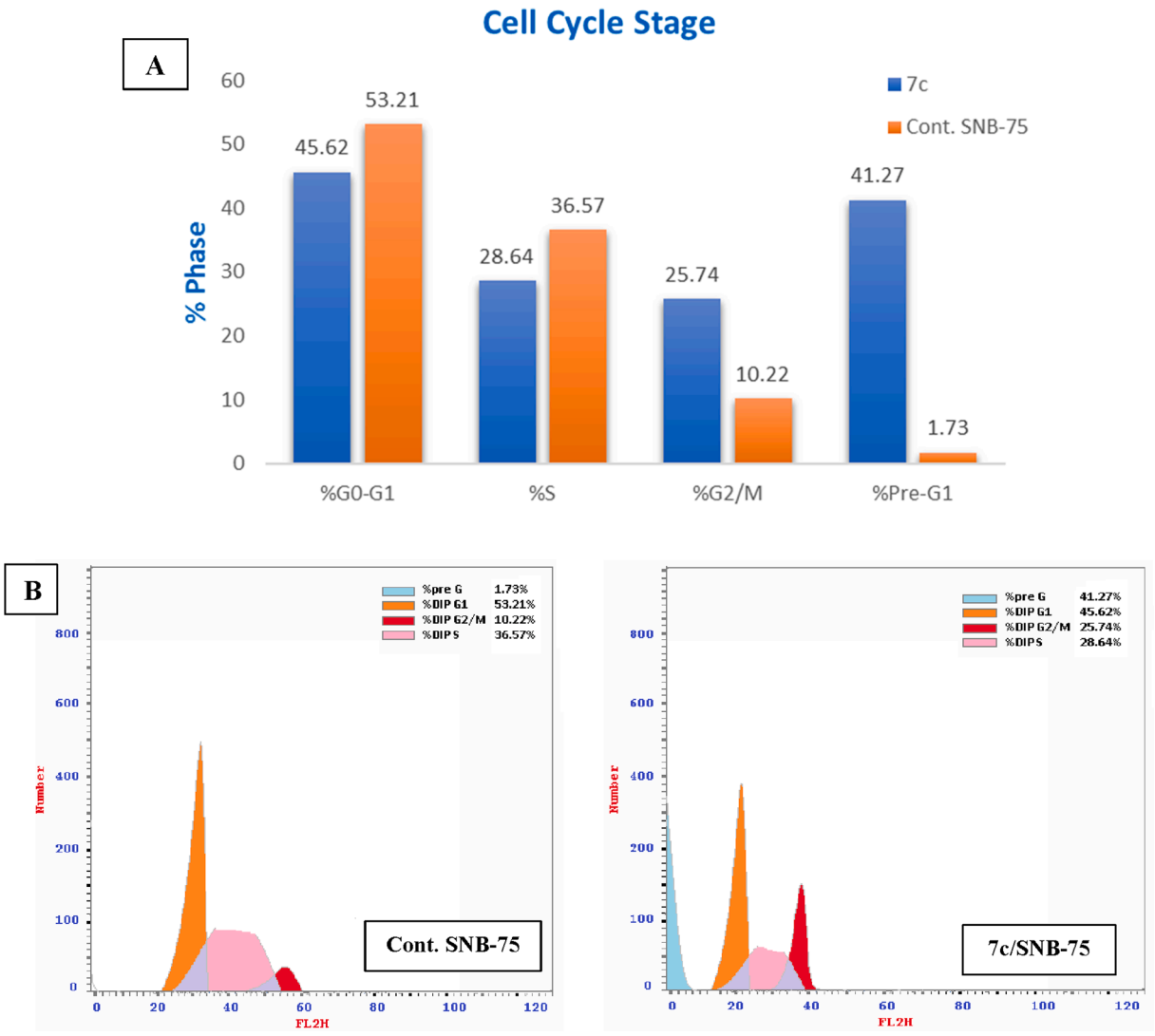

Fig. 12. A) Graphical representation of the cell cycle analysis of compound **7c**. **B)** Effect of compound **7c** (7.12 μM) on DNA-ploidy flow cytometric analysis of SNB-75 cells after 24 h.

2.2.2. *Antibacterial activity*

The antibacterial activity of the prepared compounds was evaluated *in vitro* against four pathogenic strains of both Gram-positive and Gram-negative. Gram-positive strains were represented by *Staphylococcus aureus* and *Streptococcus pneumoniae* while Gram-negative strains were represented by *Escherichia coli* and *Salmonella Typhimurium* using disc diffusion method on Muller-Hinton Agar (MHA). All tested compounds did not show any antibacterial activity against the tested bacteria.

2.2.3. *Antifungal activity*

The antifungal activity of the prepared compounds was evaluated *in vitro* against *Candida albicans*. Only compound **7d** exhibited antifungal activity against *Candida albicans* (Fig. 15) with inhibition zones of 1.8 ± 0.2, compared to an inhibition zone of 2.3 ± 0.1 cm for nystatin as the standard antifungal compound.

3. Conclusion

A series of novel thienopyrimidine-aminothiazole hybrids **7a-j** was prepared. The synthesized compounds were screened for their anti-cancer activity against the NCI-60 human tumor cell line panel. Compounds **7c** and **7d** showed broad antiproliferative activity on numerous cell lines. Compound **7c** was found to be the most potent derivative against CNS cancer cell lines SNB-75 and SF-295 and the renal cancer line CAKI-1 with IC_{50} values of 7.12 ± 0.33 and 7.36 ± 0.39 and 4.84 ± 0.22 μM, respectively. Compound **7c** showed inhibition of VEGFR-2 with IC_{50} = 62.48 ± 3.7 nM. In addition, compound **7c** lowered both total VEGFR-2 and phosphorylated VEGFR-2 in treated SNB-75 cells suggesting that **7c** has down-regulating effect on cell proliferation, growth, and survival. The results of molecular docking study confirmed that the binding pattern of compound **7c** was consistent with its VEGFR-2 inhibitory activity. The most potent compound **7c** induced significant elevation in late apoptosis phase from 0.07% to 21.3% in SNB-75 cells as shown by Annexin V-FITC/PI assay. This evidence was reinforced by an increase in the level of apoptotic caspases-3 by 9.29-fold. Moreover, analyzing the results of cell cycle analysis showed that derivative **7c** arrested the cell cycle proliferation of SNB-75 cancer cells in the G2/M phase. These results support the cytotoxic activity of **7c** and may present this compound as a candidate for further biological evaluation.

4. Experimental

4.1. *Chemistry*

4.1.1. *General*

Melting points were obtained on a Griffin apparatus and were

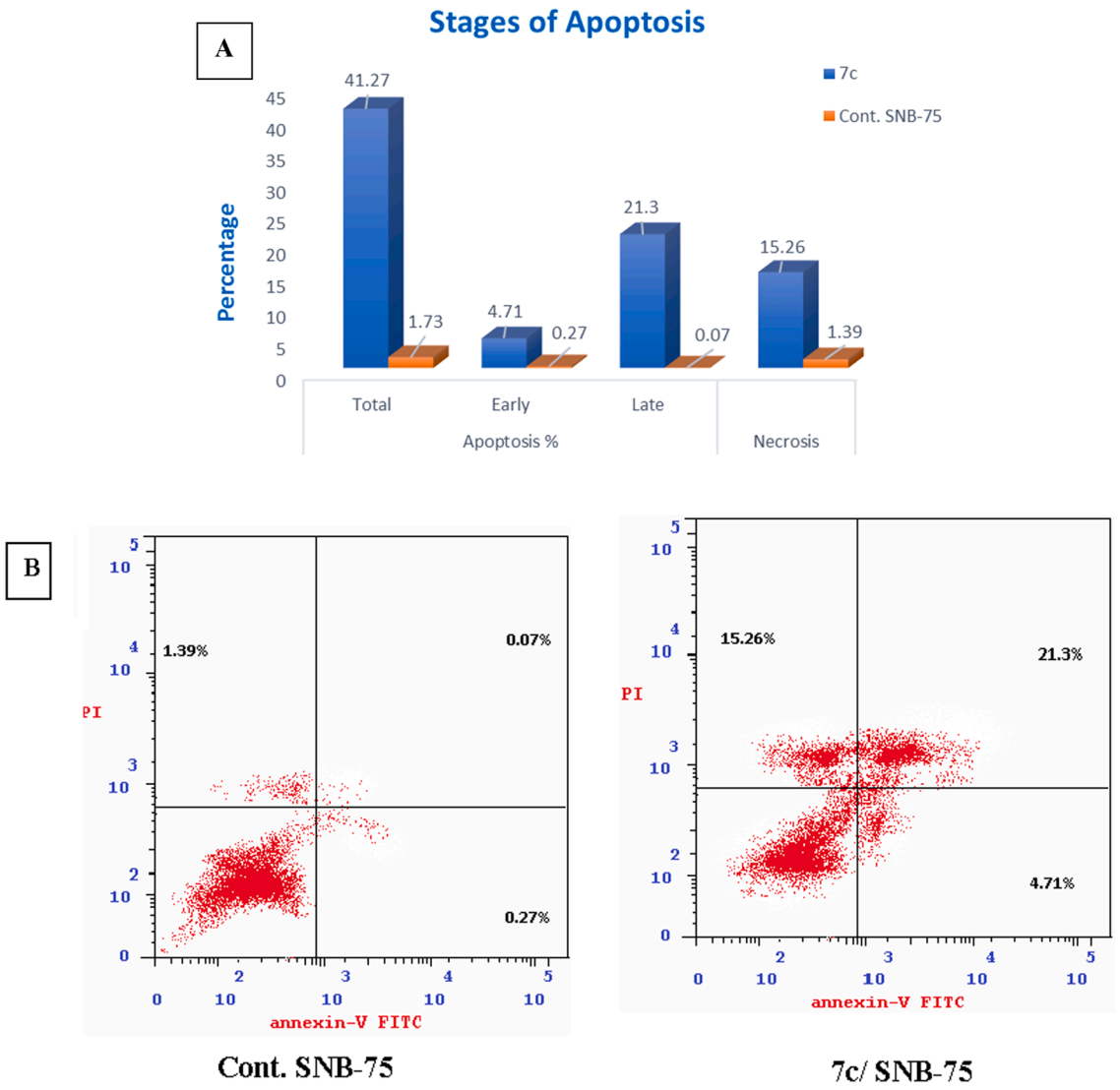

Fig. 13. A). Percentage and stages of induced apoptosis in control SNB-75 and SNB-75 treated with compound **7c**; **B)** Representative dot plots of SNB-75 cells treated with **7c** (7.12 μM) for 24 h and analyzed by flow cytometry after double staining of the cells with Annexin-V-FITC and PI.

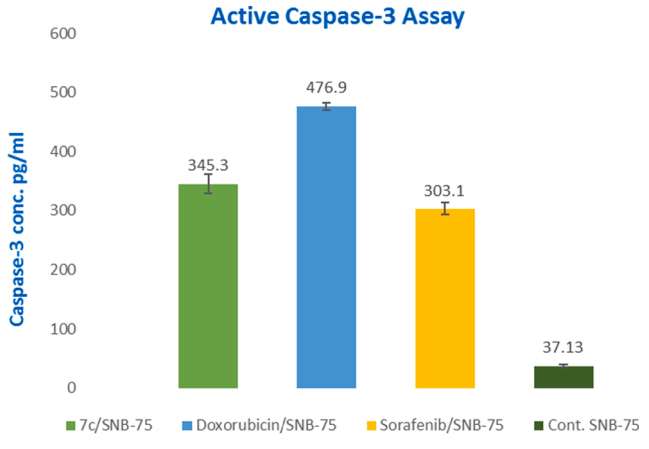

Fig. 14. Graphical representation for active caspase-3 assay of compound **7c** compared to doxorubicin and sorafenib.

uncorrected. Microanalyses for C, H and N were carried out at the Regional Center for Mycology and Biotechnology, Faculty of Pharmacy, Al-Azhar University. IR spectra were recorded on Shimadzu IR 435 spectrophotometer (Shimadzu Corp., Kyoto, Japan) Faculty of Pharmacy, Cairo University, Cairo, Egypt and values were represented in cm^{-1}. ^{1}H NMR spectra were carried out on Bruker 400 MHz (Bruker Corp., Billerica, MA, USA) spectrophotometer, Faculty of Pharmacy, Cairo University, Cairo, Egypt. Chemical shifts were recorded in ppm on δ scale, coupling constants (J) were given in Hz and peak multiplicities are designed as follows: s, singlet; d, doublet; dd, doublet of doublet; t, triplet; m, multiplet. ^{13}C NMR spectra were carried out on Bruker 100 MHz spectrophotometer, Faculty of Pharmacy, Cairo University, Cairo, Egypt. Progress of the reactions were monitored by TLC using precoated aluminum sheet silica gel MERCK 60F 254 and was visualized by UV lamp. Compounds **2a-e**, **3a-j**, **4**, **5** and **6** were prepared according to the reported procedures. [38–41]

4.1.2. General procedure for the preparation of 2-((3-(4-chlorophenyl)-4-oxo-3,4,5,6,7,8-hexahydrobenzo[4,5]thieno[2,3-d]pyrimidin-2-yl)thio)-N-(4-arylthiazol-2-yl)acetamide derivatives (7a-e) and 2-((3-(4-chlorophenyl)-4-oxo-3,4,5,6,7,8-hexahydrobenzo [4,5]thieno[2,3-d] pyrimidin-2-yl)thio)-N-(4-arylthiazol-2-yl)propanamide derivatives (7f-j)

To a solution of compound **6** (0.36 g, 0.001 mol) in absolute acetone (20 mL), derivatives **3a-j** (0.001 mol) were added. The mixture was heated under reflux for 15–20 h. The precipitate formed on hot was

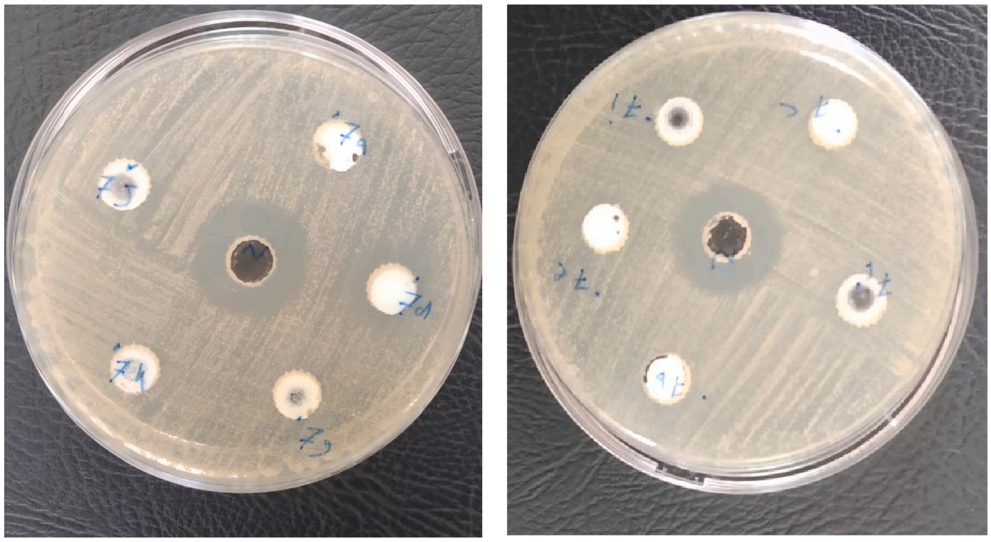

Fig. 15. Antifungal activity of the synthesized derivatives against *C. albicans* using nystatin as control.

filtered, dried and recrystallized from ethyl acetate/ ethanol mixture (1:1).

4.1.2.1. 2-((3-(4-chlorophenyl)-4-oxo-3,4,5,6,7,8-hexahydrobenzo[4,5] thieno[2,3-d]pyrimidin-2-yl)thio)-N-(4-phenylthiazol-2-yl) acetamide (7a). White solid: 75% yield; mp 170–172 °C; IR (KBr, cm^{-1}) 3298, 3113–3028, 2981–2931, 1685 (br.), 1550, 794; ^{1}H NMR (400 MHz, DMSO-d_6) δ; 12.57 (s, 1H, NH, D_2O exchangeable), 7.91 (d, J = 8.0 Hz, 2H, ArH), 7.68 (d, J = 8.8 Hz, 2H, ArH), 7.63 (s, 1H, ArH thiazole), 7.53 (d, J = 8.8 Hz, 2H, ArH), 7.45 (t, J = 8.0 Hz, 2H, ArH), 7.34 (t, J = 8.0 Hz, 1H, ArH), 4.18 (s, 2H, S-CH_2), 2.79 (t, J = 6.0 Hz, 2H, CH_2), 2.69 (t, J = 6.0 Hz, 2H, CH_2), 1.78–1.72 (m, 4H, 2CH_2); ^{13}C NMR (100 MHz, DMSO-d_6) δ: 170.7, 166.6, 161.5, 158.2, 157.6, 156.8, 149.3, 135.2, 134.9, 134.6, 131.8, 131.7, 131.3, 130.1, 129.2, 128.2, 126.1, 119.0, 108.6, 36.3, 25.5, 24.8, 22.9, 22.1. Anal. Calcd for $C_{27}H_{21}ClN_4O_2S_3$ (565.13): C, 57.38; H, 3.75; N, 9.91, found C, 57.51; H, 3.89; N, 10.12.

4.1.2.2. 2-((3-(4-chlorophenyl)-4-oxo-3,4,5,6,7,8-hexahydrobenzo[4,5] thieno[2,3-d]pyrimidin-2-yl)thio)-N-(4-(3-nitrophenyl)thiazol-2-yl)acetamide (7b). White solid: 85% yield; mp 198–200 °C; IR (KBr, cm^{-1}) 3197, 3086–3032, 2997–2843, 1681 (br.), 1562, 794; ^{1}H NMR (400 MHz, DMSO-d_6) δ; 12.71 (s, 1H, NH, D_2O exchangeable), 8.75 (s, 1H, ArH), 8.37 (d, J = 8.0 Hz, 1H, ArH), 8.19 (dd, J = 2.4, 8.0 Hz, 1H, ArH) 7.96 (s, 1H, ArH thiazole), 7.75 (t, J = 8.0 Hz, 1H, ArH), 7.68 (d, J = 8.4 Hz, 2H, ArH), 7.54 (d, J = 8.4 Hz, 2H, ArH), 4.19 (s, 2H, S-CH_2), 2.79 (t, J = 6.0 Hz, 2H, CH_2), 2.69 (t, J = 6.0 Hz, 2H, CH_2). 1.76–1.72 (m, 4H, 2CH_2), ^{13}C NMR (100 MHz, DMSO-d_6) δ: 166.9, 161.5, 158.7, 157.6, 156.7, 148.8, 146.9, 136.1, 135.2, 134.9, 132.2, 131.8, 131.3, 130.9, 130.2, 120.5, 118.9, 111.2, 36.3, 25.6, 24.8, 22.8, 22.1. Anal. Calcd for $C_{27}H_{20}ClN_5O_4S_3$ (610.13): C, 53.15; H, 3.30; N, 11.48, found C, 53.44; H, 3.62; N, 11.70.

4.1.2.3. 2-((3-(4-chlorophenyl)-4-oxo-3,4,5,6,7,8-hexahydrobenzo[4,5] thieno[2,3-d]pyrimidin-2-yl)thio)-N-(4-(4-chlorophenyl)thiazol-2-yl)acetamide (7c). Greyish white solid: 88% yield; mp 270–272 °C; IR (KBr, cm^{-1}) 3209, 3100–3074, 2935–2843, 1678 (br.), 1560, 837; ^{1}H NMR (400 MHz, DMSO-d_6) δ; 12.59 (s, 1H, NH, D_2O exchangeable), 7.93 (d, J = 8.6 Hz, 2H, ArH), 7.70 (s, 1H, ArH thiazole), 7.68 (d, J = 8.6 Hz, 2H, ArH), 7.52 (t, J = 8.8 Hz, 4H, ArH), 4.18 (s, 2H, S-CH_2), 2.79 (t, J = 6.0 Hz, 2H, CH_2), 2.69 (t, J = 6.0 Hz, 2H, CH_2), 1.78–1.73 (m, 4H, 2CH_2), ^{13}C NMR (100 MHz, DMSO-d_6) δ: 166.7, 161.5, 158.4, 157.7, 156.7, 148.1, 135.2, 134.8, 133.4, 131.7, 130.2, 129.2, 127.8, 118.9, 109.3, 36.3, 25.5, 24.8, 22.8, 22.1. Anal. Calcd for $C_{27}H_{20}Cl_2N_4O_2S_3$ (599.57): C, 54.09; H, 3.36; N, 9.34, found C, 54.23; H, 3.49; N, 9.51.

4.1.2.4. N-(4-(3-bromophenyl)thiazol-2-yl)-2-((3-(4-chlorophenyl)-4-oxo-3,4,5,6,7,8-hexahydro benzo[4,5]thieno[2,3-d]pyrimidin-2-yl) thio) acetamide (7d). White solid: 82% yield; mp 266–268 °C; IR (KBr, cm^{-1}) 3194, 3086–3001, 2935–2839, 1681 (br.), 1560, 794; ^{1}H NMR (400 MHz, DMSO-d_6) δ; 12.61 (s, 1H, NH, D_2O exchangeable), 8.12 (s, 1H, ArH), 7.92 (d, J = 8.0 Hz, 1H, ArH), 7.78 (s, 1H, ArH thiazole), 7.68 (d, J = 8.6 Hz, 2H, ArH), 7.53 (d, J = 8.6 Hz, 3H, ArH), 7.41 (t, J = 8.0 Hz, 1H, ArH), 4.18 (s, 2H, S-CH_2), 2.79 (t, J = 6.0 Hz, 2H, CH_2), 2.69 (t, J = 6.0 Hz, 2H, CH_2). 1.80–1.72 (m, 4H, 2CH_2), ^{13}C NMR (100 MHz, DMSO-d_6) δ:172.6, 166.7, 161.5, 158.4, 157.7, 156.7, 147.6, 136.8, 135.2, 134.9, 131.8, 131.4, 131.3, 130.9, 130.2, 128.7, 125.0, 122.6, 118.9, 110.1, 36.3, 25.5, 24.8, 22.8, 22.1.Anal. Calcd for $C_{27}H_{20}BrClN_4O_2S_3$ (644.03): C, 50.35; H, 3.13; N, 8.70, found C, 50.42; H, 3.38; N, 8.97.

4.1.2.5. N-(4-(4-bromophenyl)thiazol-2-yl)-2-((3-(4-chlorophenyl)-4-oxo-3,4,5,6,7,8-hexahydro benzo[4,5]thieno[2,3-d]pyrimidin-2-yl)thio) acetamide (7e). Buff solid: 98% yield; mp 258–260 °C; IR (KBr, cm^{-1}) 3213, 3100–3074, 2989–2839, 1681 (br.), 1562, 833; ^{1}H NMR (400 MHz, DMSO-d_6) δ; 12.59 (s, 1H, NH, D_2O exchangeable), 7.86 (d, J = 8.4 Hz, 2H, ArH), 7.70 (s, 1H, ArH thiazole), 7.68 (d, J = 8.4 Hz, 1H, ArH), 7.64 (d, J = 8.4 Hz, 2H, ArH), 7.61–7.58, 7.55–7.52 (m, 1H, ArH), 7.46–7.44 (m, 1H, ArH), 4.18 (s, 1H, S-CH_2), 4.16 (s, 1H, S-CH_2), 2.79 (t, J = 6.0 Hz, 2H, CH_2), 2.69 (t, J = 6.0 Hz, 2H, CH_2), 1.71–1.71 (m, 4H, 2CH_2), ^{13}C NMR (100 MHz, DMSO-d_6) δ: 166.8, 166.7, 161.5, 158.4, 157.7, 156.7, 148.1, 135.2, 134.9, 133.8, 132.1, 131.8, 130.5, 130.2, 129.7, 128.1, 121.3, 119.0, 109.4, 36.3, 25.5, 24.8, 22.9, 22.1. Anal. Calcd for $C_{27}H_{20}BrClN_4O_2S_3$ (644.03): C, 50.35; H, 3.13; N, 8.70, found C, 50.61; H, 3.40; N, 8.96.

4.1.2.6. 2-((3-(4-chlorophenyl)-4-oxo-3,4,5,6,7,8-hexahydrobenzo[4,5] thieno[2,3-d]pyrimidin-2-yl)thio)-N-(4-phenylthiazol-2-yl)propanamide (7f). Buff solid: 83% yield; mp 250–252 °C; IR (KBr, cm^{-1}) 3190, 3062–3024, 2981–2839, 1693 (br.), 1560, 793; ^{1}H NMR (400 MHz, DMSO-d_6) δ; 12.63 (s, 1H, NH, D_2O exchangeable), 7.92 (d, J = 8.0 Hz, 2H, ArH), 7.68–7.64 (m, 3H, ArH + ArH thiazole), 7.54–7.43 (m, 4H, ArH), 7.36–7.32 (m, 1H, ArH), 4.73 (q, J = 8.0 Hz, 1H, S-<u>CH</u>-CH_3), 2.78 (t, J = 6.0 Hz, 2H, CH_2), 2.69 (t, J = 6.0 Hz, 2H, CH_2), 1.79–1.70 (m, 4H, 2CH_2), 1.50 (d, J = 8.0 Hz, 3H, S-CH-<u>CH_3</u>) ^{13}C NMR (100 MHz, DMSO-d_6) δ: 170.3, 161.5, 158.1, 157.6, 156.2, 149.4, 135.2, 134.8, 134.6, 131.8, 131.7, 131.3, 130.1, 129.1, 128.2, 126.1, 119.1, 108.8,

45.9, 25.5, 24.8, 22.9, 22.1, 17.6. Anal. Calcd for $C_{28}H_{23}ClN_4O_2S_3$ (579.16): C, 58.07; H, 4.00; N, 9.67, found C, 58.24; H, 4.16; N, 9.88.

4.1.2.7. 2-((3-(4-chlorophenyl)-4-oxo-3,4,5,6,7,8-hexahydrobenzo[4,5]thieno[2,3-d]pyrimidin-2-yl)thio)-N-(4-(3-nitrophenyl)thiazol-2-yl)propanamide (7g). Yellowish white solid: 90% yield; mp 270–272 °C; IR (KBr, cm^{-1}) 3178, 3100–3074, 2981–2854, 1681 (br.), 1566, 794; ^{1}H NMR (400 MHz, DMSO-d_6) δ; 12.74 (s, 1H, NH, D_2O exchangeable), 8.77 (t, J = 4.0 Hz, 1H, ArH), 8.38–8.36 (m, 1H, ArH), 8.21–8.18 (m, 1H, ArH) 7.97 (s, 1H, ArH thiazole), 7.76 (t, J = 8.0 Hz, 1H, ArH), 7.69–7.65 (m, 2H, ArH), 7.55–7.48 (m, 2H, ArH), 4.71 (q, J = 8.0 Hz, 1H, S-CH-CH_3), 2.78 (t, J = 6.0 Hz, 2H, CH_2), 2.69 (t, J = 6.0 Hz, 2H, CH_2), 1.78–1.71 (m, 4H, $2CH_2$), 1.50 (d, J = 8.0 Hz, 3H, S-CH-CH_3) ^{13}C NMR (100 MHz, DMSO-d_6) δ: 170.6 161.4, 158.6, 157.6, 148.7, 146.9, 136.1, 135.3, 134.8, 132.1, 131.9, 131.8, 131.7, 131.3, 130.9, 130.2, 122.8, 120.5, 119.0, 111.3, 45.8, 25.5, 24.8, 22.8, 22.1, 17.3. Anal. Calcd for $C_{28}H_{22}ClN_5O_4S_3$ (624.15): Elemental Analysis: C, 53.88; H, 3.55; N, 11.22; found C, 54.16; H, 3.72; N, 11.43.

4.1.2.8. 2-((3-(4-chlorophenyl)-4-oxo-3,4,5,6,7,8-hexahydrobenzo[4,5]thieno[2,3-d]pyrimidin-2-yl)thio)-N-(4-(4-chlorophenyl)thiazol-2-yl)propanamide (7h). Buff solid: 77% yield; mp 266–268 °C; IR (KBr, cm^{-1}) 3275, 3116–3062, 2935–2839, 1681 (br.), 1590, 794; ^{1}H NMR (400 MHz, DMSO-d_6) δ; 12.64 (s, 1H, NH, D_2O exchangeable), 7.93 (d, J = 8.8 Hz, 2H, ArH), 7.70 (s, 1H, ArH thiazole), 7.68–7.64 (m, 2H, ArH), 7.54–7.47 (m, 4H, ArH), 4.71 (q, J = 7.2 Hz, 1H, S-CH-CH_3), 2.78 (t, J = 5.8 Hz, 2H, CH_2), 2.68 (t, J = 5.8 Hz, 2H, CH_2), 1.78–1.70 (m, 4H, $2CH_2$), 1.49 (d, J = 7.2 Hz, 3H, S-CH-CH_3) ^{13}C NMR (100 MHz, DMSO-d_6) δ: 170.4, 161.5, 158.3, 157.6, 156.1, 148.2, 135.2, 134.8, 133.4, 132.7, 131.8, 131.8, 131.7, 131.3, 130.2, 129.2, 127.8, 119.0, 109.5, 45.8, 25.5, 24.8, 22.9, 22.1, 17.5. Anal. Calcd for $C_{28}H_{22}Cl_2N_4O_2S_3$ (613.60): C, 54.81; H, 3.61; N, 9.13, found C, 55.08; H, 3.87; N, 9.40.

4.1.2.9. N-(4-(3-bromophenyl)thiazol-2-yl)-2-((3-(4-chlorophenyl)-4-oxo-3,4,5,6,7,8-hexa hydro benzo[4,5]thieno[2,3-d]pyrimidin-2-yl)thio) propanamide (7i). White solid: 86% yield; mp 268–270 °C; IR (KBr, cm^{-1}) 3174, 3109–3059, 2935–2839, 1693 (br.), 1573, 794; ^{1}H NMR (400 MHz, DMSO-d_6) δ; 12.64 (s, 1H, NH, D_2O exchangeable), 8.13 (s, 1H, ArH), 7.94–7.91 (m, 1H, ArH), 7.80 (s, 1H, ArH thiazole), 7.69–7.65 (m, 2H, ArH), 7.55–7.48 (m, 3H, ArH), 7.42 (t, J = 8.0 Hz, 1H, ArH), 4.71 (q, J = 8.0 Hz, 1H, S-CH-CH_3), 2.79 (t, J = 6.0 Hz, 2H, CH_2), 2.69 (t, J = 6.0 Hz, 2H, CH_2), 1.80–1.71 (m, 4H, $2CH_2$), 1.50 (d, J = 8.0 Hz, 3H, S-CH-CH_3) ^{13}C NMR (100 MHz, DMSO-d_6) δ: 170.4, 161.4, 158.3, 157.6, 156.1, 147.6, 136.8, 135.2, 134.8, 131.9, 131.8, 131.7, 131.4, 131.3, 130.9, 130.2, 128.7, 124.9, 122.6, 119.0, 110.3, 45.8, 25.5, 24.8, 22.8, 22.1, 17.4. Anal. Calcd for $C_{28}H_{22}BrClN_4O_2S_3$ (658.05): C, 51.11; H, 3.37; N, 8.51, found C, 51.34; H, 3.53; N, 8.79.

4.1.2.10. N-(4-(4-bromophenyl)thiazol-2-yl)-2-((3-(4-chlorophenyl)-4-oxo-3,4,5,6,7,8-hexa hydrobenzo[4,5]thieno[2,3-d]pyrimidin-2-yl)thio) propanamide (7j). White solid: 67% yield; mp 250–252 °C; IR (KBr, cm^{-1}) 3275, 3107–3062, 2935–2839, 1685 (br.), 1546, 794; ^{1}H NMR (400 MHz, DMSO-d_6) δ; 12.64 (s, 1H, NH, D_2O exchangeable), 7.87 (d, J = 8.0 Hz, 2H, ArH), 7.72 (s, 1H, ArH thiazole), 7.68–7.63 (m, 4H, ArH), 7.54–7.47 (m, 2H, ArH), 4.71 (q, J = 7.2 Hz, 1H, S-CH-CH_3), 2.78 (t, J = 6.0 Hz, 2H, CH_2), 2.69 (t, J = 6.0 Hz, 2H, CH_2), 1.78–1.71 (m, 4H, $2CH_2$), 1.49 (d, J = 7.2 Hz, 3H, S-CH-CH_3) ^{13}C NMR (100 MHz, DMSO-d_6) δ: 170.4, 161.5, 158.3, 157.6, 156.1, 148.2, 135.2, 134.8, 133.8, 132.1, 131.8, 131.7, 131.7, 131.3, 130.2, 128.1, 121.3, 119.0, 109.6, 45.8, 25.5, 24.8, 22.8, 22.1, 17.5. Anal. Calcd for $C_{28}H_{22}BrClN_4O_2S_3$ (658.05): C, 51.11; H, 3.37; N, 8.51, found C, 51.40; H, 3.52; N, 8.78.

4.2. Biological testing

4.2.1. Anticancer activity

4.2.1.1. Measurement of anticancer activity against a panel of 60 cell lines. Screening of the anticancer activity of the newly synthesized compounds **7a-j** was performed by the US National Cancer Institute (NCI) using 60 different human tumor cell lines as in accordance with the standard procedure as formerly reported [43–46]. In brief, 100 μL of each cell type were inoculated into 96 well microplates which were then incubated at 37 °C, 5% CO_2, 95% air and 100% relative humidity for 24 h. Two plates of each cell line were fixed in situ with TCA and constitutes the cell population measurement at zero time (Tz). Tested compounds were dissoluted in dimethyl sulfoxide and were added to the microplate wells containing 100 μL of complete medium with 50 mg/mL gentamicin and the plates were then incubated for 48 h at 37 °C, 5% CO_2, 95% air, and 100% relative humidity. For adherent cells, the experiment was ended and cells were fixed by adding 50 μL of cold 50% (w/v) TCA with incubation at 4 °C for 60 min. The supernatant was removed, and plates were washed five times with tap water and air dried. Then, 100 μL of 0.4% (w/v) sulforhodamine B (SRB) solution in 1% acetic acid was added to all wells, and plates were incubated for 10 min at room temperature. Later, unbound dye was washed away five times with 1% acetic acid and the plates were air dried. Bound stain was then dissolved in 10 mM trizma base, and the absorbance was measured at 515 nm using an automated microplate reader. For suspension cells, the same procedure is carried out except that the experiment was ended by fixing settled cells at the bottom of the wells by adding 50 μL of 80% TCA. Calculation of growth inhibition percentages was as follows:

$$[(\mathrm{Ti}-\mathrm{Tz})/(\mathrm{C}-\mathrm{Tz})]\times 100 \text{ for concentrations for which } \mathrm{Ti}\geq \mathrm{Tz}$$

$$[(\mathrm{Ti}-\mathrm{Tz})/\mathrm{Tz}]\times 100 \text{ for concentrations for which } \mathrm{Ti}< \mathrm{Tz}$$

Where, (Tz) is the absorbance at time zero, (C) is the absorbance of control growth, and (Ti) is the absorbance of test after the addition of the drug. The one-dose data are reported as a mean graph of the percent growth of treated cells. The reported number is growth relative to the no-compound control and relative to the time zero number of cells. This permits recognition of both growth inhibition and lethality.

4.2.1.2. In vitro anti-proliferative activity

4.2.1.2.1. Cell culture. Cell line cells were obtained from American Type Culture Collection, cells and were cultured using Dulbecco's Modified Eagle's Medium (DMEM) (Invitrogen/Life Technologies) supplemented with 10% fetal bovine serum (FBS) (Hyclone), 10 μg/mL of insulin (Sigma), and 1% penicillin–streptomycin. All of the added chemicals and reagents were obtained from Sigma, or Invitrogen. Plate cells (cells density 1.2–1.8 × 10,000 cells/well) in a volume of 100 μL complete growth medium and 100 μL of the tested compound per well in a 96-well plate for 24 h before the MTT assay.

4.2.1.2.2. Cell culture protocol. Culture medium was removed to a centrifuge tube. The cell layer was rinsed with 0.25% (w/v) Trypsin 0.53 μM ethylenediaminetetraacetic acid (EDTA) solution to eliminate all traces of serum which contains Trypsin inhibitor. Trypsin EDTA solution (2.0–3.0 mL) was added to flask and cells were observed under an inverted microscope until cell layer is dispersed. Growth medium (6.0–8.0 mL) was added and cells were aspirated by gently pipetting. The cell suspension was transferred to the centrifuge tube with the medium and was centrifuged for 5–10 min. The supernatant was discarded. The cell pellet was suspended in new growth medium. Appropriate aliquots of the cell suspension were added to new culture vessels. Cultures were incubated at 37 °C for 24 h. After treatment of cells with the serial concentrations of the compound to be tested incubation is carried out for 48 h at 37 °C, then the plates were examined under the inverted microscope and were preceded for the MTT assay.

4.2.1.2.3. MTT assay protocol. The 3-(4,5-dimethylthiazol-2-yl)-2,5-diphenyltetrazolium bromide (MTT) method [47] of monitoring *in vitro* cytotoxicity is suitable for use with multiwell plates. The evaluation of cell population growth is based on the capability of living cells to reduce the yellow product MTT to a blue product, formazan, by a reduction reaction occurring in the mitochondria. The three cell lines were incubated for 24 h in 96-microwell plates. The number of living cells in the presence or absence (control) of the various test compounds is directly proportional to the intensity of the blue color, measured by spectrophotometry using (ROBONIK P2000 Spectrophotometer) at a wavelength of 570 nm. Measure the background absorbance of multiwell plates at 690 nm and subtract from the 570 nm measurement. Five concentrations ranging from 0.01 μM to 100 μM (with semi-log decrease in concentration) were tested for each of the compounds under study. Each experiment was carried out in triplicate. The IC_{50} values [the concentration required for 50% inhibition of cell viability] were calculated using sigmoidal dose response curve-fitting models.

4.2.1.3. Measurement of inhibitory activity against VEGFR-2. In vitro VEGFR-2 inhibitory activity of compounds **7c**, **7d** and **7e** was evaluated using ten-fold serial dilutions (1, 0.1, 0.01, 0.001 μM) against VEGFR-2 (KDR) Kinase Assay Kit Catalog # 40,325 according to the manufacturer's instructions. Briefly, the master mixture (25 μL per well) was prepared and added to each well. 5 μL of inhibitor solution of each well labeled as "Test Inhibitor" was added. For the "Positive Control" and "Blank", 5 μL of the same solution without inhibitor (Inhibitor buffer) was added. 3 mL of kinase buffer was prepared by mixing 600 μL of kinase buffer with 2400 μL water. To the wells designated as "Blank", 20 μL of kinase buffer was added. The amount of VEGFR-2 needed for the assay was calculated and diluted to 1 ng/μL with kinase buffer. The reaction was initiated by adding 20 μL of diluted VEGFR-2 to the wells labelled "Positive Control" and "Test Inhibitor Control". The mixtures were incubated at 30 °C for 45 min. After the 45 min, 50 μL of Kinase-Glo Max reagent was added to each well. The plate was incubated at room temperature for 15 min. Luminescence was measured using the microplate reader.

4.2.1.4. Measurement of total VEGFR-2 concentration. The effect of compound **7c** on total VEGFR-2 expression in SNB-75 CNS cancer cell line was evaluated at the IC_{50} of compound **7c** (7.12 μM) using Human VEGF Receptor 2 Simple Step ELISA (Enzyme-Linked Immunosorbent Assay) Kit according to the manufacturer's instructions. Briefly the assay in 96-well plates employs an affinity tag labelled capture antibody and a reporter conjugated detector antibody which immunocapture the sample analyte in solution. The complex (captured antibody/analyte/detector antibody) is, in turn, immobilized via immunoaffinity of an anti-tag antibody coating the well. The concentration of total VEGFR-2 was measured by recoding the OD at 450 nm followed by quantification using the standard curve.

4.2.1.5. Measurement of phosphorylated VEGFR-2. The ability of compound **7c** to inhibit VEGFR-2 phosphorylation in SNB-75 cells was performed using VEGFR-2 (Phospho-Tyr951) Colorimetric Cell-Based ELISA Kit, Aviva Systems Biology Corporation San Diego, USA (Catalog #: OKAG02083) according to the manufacturer's directions.

4.2.1.6. Molecular docking of the active compounds in the active site of VEGFR-2. All the molecular modeling studies were carried out using Molecular Operating Environment (MOE, 2019.0102) software. All minimizations were performed with MOE until an RMSD gradient of 0.05 kcal•$mol^{-1}Å^{-1}$ with MMFF94x force field and the partial charges were automatically calculated. The X-ray crystallographic structure of vascular endothelial growth factor receptor 2 (VEGFR-2) co-crystalized with sorafenib (**PDB ID: 4ASD**) [50] was downloaded from the protein data bank [51]. For each co-crystallized enzyme; water molecules and ligands which are not involved in the binding were removed, the protein was prepared for the docking study using *Protonate 3D* protocol in MOE with default options. The co-crystalized ligand (sorafeinib) was used to define the binding site for docking. Triangle Matcher placement method and London dG scoring function were used for docking.

4.2.1.7. Measurement of the effect of compound 7c on the level of caspase-3 protein (Marker of apoptosis). The level of the apoptotic marker caspase-3 was measured using BIORAD iScript TM One-Step RT-PCR kit with SYBR® Green. The procedure of the used kit was performed according to the manufacturer's instructions.

4.2.1.7.1. RNA isolation and reverse transcription. mRNA isolation is carried out using RNeasy extraction kit, up to 1 × 107 cells, depending on the cell line. Cells are disrupted in RNeasy Lysis Buffer (RLT buffer) and homogenized, ethanol is then added to the lysate, generating conditions that stimulate selective binding of RNA to the RNeasy membrane. The sample is then applied to the RNeasy mini spin column, total RNA binds to the membrane, contaminants are efficiently flew through, and high quality RNA is eluted in RNase-free water.

4.2.1.7.2. Master mix preparation. All the following reagents were mixed together to give total volume (50 μL). 2X SYBR® Green RT-PCR reaction mixture (25 μL), forward primer (10 μM) (1.5 μL), reverse primer (10 μM) (1.5 μL), nuclease-free H_2O (11 μL), RNA template (1 pg to 100 ng total RNA) (10 μL) and iScript reverse transcriptase for One-Step RT-PCR (1 μL).

4.2.1.7.3. Amplification protocol. Incubate whole reaction mixture in a real-time thermal detection system (Rotorgene) as follows: cDNA synthesis: 10 min at 50 °C, iScript reverse transcriptase inactivation: 5 min at 95 °C, polymerase chain reaction (PCR) cycling and detection (30–45 cycles): 10 s at 95 °C and 30 s at 55 °C to 60 °C (data collection step) and melt curve analysis: 1 min at 95 °C and 1 min at 55 °C and 10 s at 55 °C (80 cycles, increasing each by 0.5 °C each cycle).

4.2.1.8. Cell cycle analysis of compound 7c. The SNB-75 cells were treated with compound **7c** at its IC_{50} concentration for 24 h. After treatment, the cells were then washed with ice-cold phosphate buffered saline (PBS) twice, collected by centrifugation and fixed at −20 °C in 70% (v/v) ethanol, washed with PBS, re-suspended with 0.1 mg/mL RNase, stained with 40 mg/mL propidium iodide (PI), incubated for 1 h and analyzed by flow cytometry using FACS Calibur (Becton Dickinson) [52]. The cell cycle distributions were calculated using Cell- Quest software (Becton Dickinson).

4.2.1.9. Measurement of apoptosis using Annexin-V-FITC apoptosis detection kit. Annexin V fluorescein isothiocyanate (FITC) /PI apoptosis detection kit (BD Biosciences, San Diego, CA) was used according to the manufacturer's instructions to measure the apoptotic activity of compounds **7c**. Briefly, 4×10^6 cell/T 75 flask were exposed to compound **7c** at its IC_{50} concentration for 24 h. The cells then were collected by trypsinization and 0.5×10^6 cells were washed twice with PBS and stained with 5 μL Annexin V-FITC and 5 μL PI in 1 × binding buffer for 15 min at room temperature in the dark. Annexin V-FITC binding was analyzed using a BD FACS Calibur flow cytometer (BD Biosciences, San Jose, CA).

4.2.2. Antibacterial activity

The antibacterial activity of the prepared compounds **7a-j** was evaluated *in vitro* against four pathogenic strains of both Gram-positive and Gram-negative using disc diffusion method on Muller-Hinton Agar (MHA). Gram-positive strains were represented by *Staphylococcus aureus* and *Streptococcus pneumoniae* while Gram-negative strains were represented by *Escherichia coli* and *Salmonella Typhimurium*.

The test organisms were maintained on agar slant at 4 °C and subcultured on a fresh agar plates. For disc diffusion assay, bacterial liquid cultures were initiated by placing a loop of bacteria from the slant into

10 mL of Lysogeny Broth (LB) medium [53]. Agar diffusion test was conducted to detect the bacterial susceptibility to the prepared compounds. A volume of 100 μL of cell culture suspension matching with 0.5 McFarland of each test organism were spread onto the surface of MHA medium. The prepared compounds were adjusted to a concentration of 50 mg/mL using DMSO as a solvent. Filter paper discs with a diameter of 7 mm each were impregnated with 15 μL of each of the different compounds. Then the agar plates containing microorganisms, soaked with paper discs (5 μg) were incubated at 37 ± 0.1 °C for 24 h to allow bacterial growth. After incubation, the inhibition of bacterial growth was evaluated by measuring the diameter (cm) of the clear zone around each disc. The resulting inhibition zones were compared with the inhibition zones of the standard antibiotics Ampicillin (AM-10) and Levofloxacin (LEV-5). Filter paper discs impregnated with 15 μL of DMSO were also used as control for the solvent. The experiment was carried out in triplicates for statistical relevance and the Mean ± SE of results was calculated.

4.2.3. Antifungal activity

The antifungal activity of the prepared compounds **7a-j** was evaluated *in vitro* against *Candida albicans NRRL-Y 477*. Well diffusion method was conducted to detect the *C. albicans* susceptibility to the prepared compounds [54]. The test organism was maintained on Sabouraud Dextrose Agar (SDA) slant at 4 °C. The prepared compounds were adjusted to a concentration of 50 mg/mL using DMSO as a solvent. For well diffusion assay, an inoculum was subcultured on SDA plate and the plate was incubated for 24 h at 35 °C. One colony obtained from agar was inoculated into Sabouraud Dextrose broth followed by incubation at 35 °C to prepare a suspension of a concentration matching 0.5 McFarland standard. A total of 1 mL of the prepared suspension was swabbed on Potato Dextrose Agar (PDA) plate and left to dry. Wells with a diameter of 4 mm were cut out of the agar, and a total of 50 μL of each of the prepared compounds was placed is a separate well. The plates were then incubated at 35 ± 0.1 °C for 48 h to allow fungal growth. After incubation, the inhibition of fungal growth was evaluated by measuring the diameter (cm) of the clear zone around each well. The resulting inhibition zones were compared with the inhibition zones of a well containing 50 μL of Nystatin (1000 IU/ ml) suspension as the standard antifungal compound. A well containing 50 μL of DMSO was also used as control for the solvent. The experiment was carried out in triplicates for statistical relevance and the Mean ± SE of results was calculated.

Declaration of Competing Interest

The authors declare that they have no known competing financial interests or personal relationships that could have appeared to influence the work reported in this paper.

Acknowledgments

The authors are grateful to all associates of National Institutes of Health, USA for carrying out the anticancer screening. The authors thank Dr. Esam Rashwan, Head of the confirmatory diagnostic unit VACSERA-EGYPT, for carrying out cell cycle analysis, VEGFR-2 assays and caspase-3 marker.

Appendix A. Supplementary material

Supplementary data to this article can be found online at https://doi.org/10.1016/j.bioorg.2021.105137.

References

[1] J. Folkman, Tumor angiogenesis: therapeutic implications, N. Engl. J. Med. 285 (1971) 1182–1186.
[2] K. Zirlik, J. Duyster, Anti-Angiogenics: Current Situation and Future Perspectives, Oncol. Res. Treat. 41 (2018) 166–171, https://doi.org/10.1159/000488087.
[3] Z.K. Otrock, J.A. Makarem, A.I. Shamseddine, Vascular endothelial growth factor family of ligands and receptors: Review, Blood Cells, Mol. Dis. 38 (2007) 258–268, https://doi.org/10.1016/j.bcmd.2006.12.003.
[4] F. Musumeci, M. Radi, C. Brullo, S. Schenone, Vascular endothelial growth factor (VEGF) receptors: Drugs and new inhibitors, J. Med. Chem. 55 (2012) 10797–10822, https://doi.org/10.1021/jm301085w.
[5] A. Seeber, E. Gunsilius, G. Gastl, A. Pircher, Anti-Angiogenics: Their Value in Colorectal Cancer Therapy, Oncol. Res. Treat. 41 (2018) 188–193, https://doi.org/10.1159/000488301.
[6] R.J. Arai, V. Petry, P.M. Hoff, M.S. Mano, Serum levels of VEGF and MCSF in HER2 + / HER2- breast cancer patients with metronomic neoadjuvant chemotherapy, Biomark. Res. 6 (2018) 1–6, https://doi.org/10.1186/s40364-018-0135-x.
[7] M. Janning, S. Loges, Anti-Angiogenics: Their Value in Lung Cancer Therapy, Oncol. Res. Treat. 41 (2018) 172–180, https://doi.org/10.1159/000488119.
[8] B.I. Rini, VEGF-targeted therapy in renal cell carcinoma: Active drugs and active choices, Curr. Oncol. Rep. 8 (2006) 85–89, https://doi.org/10.1007/s11912-006-0041-5.
[9] R.K. Jain, E. Di Tomaso, D.G. Duda, J.S. Loeffler, A.G. Sorensen, T.T. Batchelor, Angiogenesis in brain tumours, Nat. Rev. Neurosci. 8 (2007) 610–622, https://doi.org/10.1038/nrn2175.
[10] A. Parveen, L. Subedi, H. Kim, Z. Khan, Z. Zahra, M. Farooqi, S. Kim, Phytochemicals Targeting VEGF and VEGF-Related Multifactors as Anticancer Therapy, J. Clin. Med. 8 (2019) 350, https://doi.org/10.3390/jcm8030350.
[11] P. Wu, T.E. Nielsen, M.H. Clausen, FDA-approved small-molecule kinase inhibitors, Trends Pharmacol. Sci. 36 (2015) 422–439, https://doi.org/10.1016/j.tips.2015.04.005.
[12] Q.Q. Xie, H.Z. Xie, J.X. Ren, L.L. Li, S.Y. Yang, Pharmacophore modeling studies of type I and type II kinase inhibitors of Tie2, J. Mol. Graph. Model. 27 (2009) 751–758, https://doi.org/10.1016/j.jmgm.2008.11.008.
[13] V.A. Machado, D. Peixoto, R. Costa, H.J.C. Froufe, R.C. Calhelha, R.M.V. Abreu, I. C.F.R. Ferreira, R. Soares, M.J.R.P. Queiroz, Synthesis, antiangiogenesis evaluation and molecular docking studies of 1-aryl-3-[(thieno[3,2-b]pyridin-7-ylthio)phenyl] ureas: Discovery of a new substitution pattern for type II VEGFR-2 Tyr kinase inhibitors, Bioorganic Med. Chem. 23 (2015) 6497–6509, https://doi.org/10.1016/j.bmc.2015.08.010.
[14] A. Ghith, K.M. Youssef, N.S.M. Ismail, K.A.M. Abouzid, Design, synthesis and molecular modeling study of certain VEGFR-2 inhibitors based on thienopyrimidne scaffold as cancer targeting agents, Bioorg. Chem. 83 (2019) 111–128, https://doi.org/10.1016/j.bioorg.2018.10.008.
[15] K. El-Adl, A.G.A. El-Helby, H. Sakr, S.S.A. El-Hddad, Design, synthesis, molecular docking, and anticancer evaluations of 1-benzylquinazoline-2,4(1H,3H)-dione bearing different moieties as VEGFR-2 inhibitors, Arch. Pharm. (Weinheim). 353 (2020), e2000068, https://doi.org/10.1002/ardp.202000068.
[16] J. Dietrich, C. Hulme, L.H. Hurley, The design, synthesis, and evaluation of 8 hybrid DFG-out allosteric kinase inhibitors: A structural analysis of the binding interactions of Gleevec ®, Nexavar®, and BIRB-796, Bioorganic Med. Chem. 18 (2010) 5738–5748, https://doi.org/10.1016/j.bmc.2010.05.063.
[17] A. Garofalo, L. Goossens, P. Six, A. Lemoine, S. Ravez, A. Farce, P. Depreux, Impact of aryloxy-linked quinazolines: A novel series of selective VEGFR-2 receptor tyrosine kinase inhibitors, Bioorganic Med. Chem. Lett. 21 (2011) 2106–2112, https://doi.org/10.1016/j.bmcl.2011.01.137.
[18] E.M.H. Ali, M.S. Abdel-Maksoud, C.H. Oh, Thieno[2,3-d]pyrimidine as a promising scaffold in medicinal chemistry: Recent advances, Bioorganic Med. Chem. 27 (2019) 1159–1194, https://doi.org/10.1016/j.bmc.2019.02.044.
[19] A. Faraji, T. Oghabi Bakhshaiesh, Z. Hasanvand, R. Motahari, E. Nazeri, M.A. Boshagh, L. Firoozpour, H. Mehrabi, A. Khalaj, R. Esmaeili, A. Foroumadi, Design, synthesis and evaluation of novel thienopyrimidine-based agents bearing diaryl urea functionality as potential inhibitors of angiogenesis, Eur. J. Med. Chem. 209 (2021) 112942. https://doi.org/10.1016/j.ejmech.2020.112942.
[20] M.A. Khedr, K.M. Abu-Zied, W.A. Zaghary, A.S. Aly, D.N. Shouman, H. Haffez, Novel thienopyrimidine analogues as potential metabotropic glutamate receptors inhibitors and anticancer activity: Synthesis, In-vitro, In-silico, and SAR approaches, Bioorg. Chem. 109 (2021), 104729, https://doi.org/10.1016/j.bioorg.2021.104729.
[21] K. Nagaraju, V.H.S.S. Bhaskaruni, R. Kishore, S. Maddila, P. Singh, S. B. Jonnalagadda, Synthesis and antioxidant evaluation of a new class of thienopyrimidinerhodanine hybrids, Lett. Drug Des. Discov. 15 (2018) 118–126, https://doi.org/10.2174/1570180814666170710161844.
[22] M.S. Tolba, A.M. Kamal El-Dean, M. Ahmed, R. Hassanien, Synthesis, reactions, and biological study of some new thienopyrimidine derivatives as antimicrobial and anti-inflammatory agents, J. Chinese Chem. Soc. 66 (2019) 548–557, https://doi.org/10.1002/jccs.201800292.
[23] A.F. Saber, M. Sayed, M.S. Tolba, A.M. Kamal El-Dean, R. Hassanien, M. Ahmed, A facile method for preparation and evaluation of the antimicrobial efficiency of various heterocycles containing thieno[2,3-d]pyrimidine, Synth. Commun. 51 (2021) 398–409, https://doi.org/10.1080/00397911.2020.1829645.
[24] A. Bassetto, M., Leyssen, P., Neyts, J., Yerukhimovich, M. M., Frick, D. N., Brancale, Computer-aided identification, synthesis and evaluation of substituted thienopyrimidines as novel inhibitors of HCV replication, 123 (2016) 31–47. https://doi.org/10.1016/j.ejmech.2016.07.035.
[25] S.-G. Li, C. Vilchèze, S. Chakraborty, X. Wang, H. Kim, M. Anisetti, S. Ekins, K. Y. Rhee, W.R. Jacobs Jr, J.S. Freundlich, Evolution of a thienopyrimidine antitubercular relying on medicinal chemistry and metabolomics insights, Tetrahedron Lett. 56 (2015) 3246–3250, https://doi.org/10.1016/j.tetlet.2015.02.129.

[26] J. Kankanala, K.A. Kirby, A.D. Huber, M.C. Casey, D.J. Wilson, S.G. Sarafianos, Z. Wang, Design, synthesis and biological evaluations of N-Hydroxy thienopyrimidine-2,4-diones as inhibitors of HIV reverse transcriptase-associated RNase H, Eur. J. Med. Chem. 141 (2017) 149–161, https://doi.org/10.1016/j.ejmech.2017.09.054.
[27] L.D. Jennings, S.L. Kincaid, Y.D. Wang, G. Krishnamurthy, C.F. Beyer, J. P. McGinnis, M. Miranda, C.M. Discafani, S.K. Rabindran, Parallel synthesis and biological evaluation of 5,6,7,8- tetrahydrobenzothieno[2,3-d]pyrimidin-4(3H)-one cytotoxic agents selective for p21-deficient cells, Bioorganic Med. Chem. Lett. 15 (2005) 4731–4735, https://doi.org/10.1016/j.bmcl.2005.07.072.
[28] A.S. El-Azab, M.A. Al-Omar, A.A.M. Abdel-Aziz, N.I. Abdel-Aziz, M.A.A. El-Sayed, A.M. Aleisa, M.M. Sayed-Ahmed, S.G. Abdel-Hamide, Design, synthesis and biological evaluation of novel quinazoline derivatives as potential antitumor agents: Molecular docking study, Eur. J. Med. Chem. 45 (2010) 4188–4198, https://doi.org/10.1016/j.ejmech.2010.06.013.
[29] I.M. Elfekki, W.F.M. Hassan, H.E.A.E. Elshihawy, I.A.I. Ali, E.H.M. Eltamany, Molecular modeling studies and synthesis of novel methyl 2-(2-(4-Oxo-3-aryl-3,4-dihydroquinazolin-2-ylthio)acetamido)alkanoates with potential anti-cancer activity as inhibitors for methionine synthase, Chem. Pharm. Bull. 62 (2014) 675–694, https://doi.org/10.1248/cpb.c14-00158.
[30] A. Lilienkampf, S. Karkola, S. Alho-Richmond, P. Koskimies, N. Johansson, K. Huhtinen, K. Vihko, K. Wähälä, Synthesis and biological evaluation of 17β-hydroxysteroid dehydrogenase type 1 (17β-HSD1) inhibitors based on a thieno [2,3-d] pyrimidin-4(3H)-one core, J. Med. Chem. 52 (2009) 6660–6671, https://doi.org/10.1021/jm900928k.
[31] H. Nara, K. Sato, T. Naito, H. Mototani, H. Oki, Y. Yamamoto, H. Kuno, T. Santou, N. Kanzaki, J. Terauchi, O. Uchikawa, M. Kori, Thieno[2,3-d]pyrimidine-2-carboxamides bearing a carboxybenzene group at 5-position: Highly potent, selective, and orally available MMP-13 inhibitors interacting with the S1″ binding site, Bioorganic Med. Chem. 22 (2014) 5487–5505, https://doi.org/10.1016/j.bmc.2014.07.025.
[32] H.G. Häcker, A. de la Haye, K. Sterz, G. Schnakenburg, M. Wiese, M. Gütschow, Analogs of a 4-aminothieno[2,3-d]pyrimidine lead (QB13) as modulators of P-glycoprotein substrate specificity, Bioorganic Med. Chem. Lett. 19 (2009) 6102–6105, https://doi.org/10.1016/j.bmcl.2009.09.023.
[33] E.F. Abdelhaleem, M.K. Abdelhameid, A.E. Kassab, M.M. Kandeel, Design and synthesis of thienopyrimidine urea derivatives with potential cytotoxic and pro-apoptotic activity against breast cancer cell line MCF-7, Eur. J. Med. Chem. 143 (2018) 1807–1825, https://doi.org/10.1016/j.ejmech.2017.10.075.
[34] M.A. Aziz, R.A.T. Serya, D.S. Lasheen, A.K. Abdel-Aziz, A. Esmat, A.M. Mansour, A. N.B. Singab, K.A.M. Abouzid, Discovery of Potent VEGFR-2 Inhibitors based on Furopyrimidine and Thienopyrimidne Scaffolds as Cancer Targeting Agents, Sci. Rep. 6 (2016) 24460, https://doi.org/10.1038/srep24460.
[35] P.C. Sharma, K.K. Bansal, A. Sharma, D. Sharma, A. Deep, Thiazole-containing compounds as therapeutic targets for cancer therapy, Eur. J. Med. Chem. 188 (2020), 112016, https://doi.org/10.1016/j.ejmech.2019.112016.
[36] M.S.H. Salem, Y.M. Abdel Aziz, M.S. Elgawish, M.M. Said, K.A.M. Abouzid, Design, synthesis, biological evaluation and molecular modeling study of new thieno[2,3-d]pyrimidines with anti-proliferative activity on pancreatic cancer cell lines, Bioorg. Chem. 94 (2020), 103472, https://doi.org/10.1016/j.bioorg.2019.103472.
[37] L.M. Zhao, T.P. Xie, Y.Q. He, D.F. Xu, S.S. Li, Synthesis and antitumor activity of 6- and 2-(1-substituted-thio-4-methylpent-3-enyl)-5,8-dimethoxynaphthalene-1,4-diones, Eur. J. Med. Chem. 44 (2009) 1410–1414, https://doi.org/10.1016/j.ejmech.2008.09.039.
[38] G. Yan, L. Hao, Y. Niu, W. Huang, W. Wang, F. Xu, L. Liang, C. Wang, H. Jin, P. Xu, 2-Substituted-thio-N-(4-substituted-thiazol/1H-imidazol-2-yl)acetamides as BACE1 inhibitors: Synthesis, biological evaluation and docking studies, Eur. J. Med. Chem. 137 (2017) 462–475, https://doi.org/10.1016/j.ejmech.2017.06.020.
[39] X. Li, X. Zhou, J. Zhang, L. Wang, L. Long, Z. Zheng, S. Li, W. Zhong, Synthesis and Biological Evaluation of Chromenylurea and Chromanylurea Derivatives as Anti-TNF-a agents that Target the p38 MAPK Pathway, Molecules 19 (2014) 2004–2028, https://doi.org/10.3390/molecules19022004.
[40] A.P. Peet, N. P., Sunder, S., Barbuch, R. J., & Vinogradoff, (1986). Mechanistic observations in the gewald syntheses of 2-aminothiophenes, J. Heterocycl. Chem. 23 (1986) 129–134.
[41] K.M. Al-Taisan, H.M.A. Al-Hazimi, S.S. Al-Shihry, Synthesis, characterization and biological studies of some novel thieno[2,3-d]pyrimidines, Molecules 15 (2010) 3932–3957, https://doi.org/10.3390/molecules15063932.
[42] National Cancer Institute – Developmental Therapeutics Program, (n.d.). www.dtp.nci.nih.gov.
[43] M.R. Boyd, K.D. Paull, Some practical considerations and applications of the national cancer institute in vitro anticancer drug discovery screen, Drug Dev. Res. 34 (1995) 91–109, https://doi.org/10.1002/ddr.430340203.
[44] R.H. Shoemaker, The NCI60 human tumour cell line anticancer drug screen, Nat. Rev. Cancer. 6 (2006) 813–823, https://doi.org/10.1038/nrc1951.
[45] P. Skehan, R. Storeng, D. Scudiero, A. Monks, J. Mcmahon, D. Vistica, J.T. Warren, H. Bokesch, S. Kenney, M.R. Boyd, New colorimetric cytotoxicity assay for anticancer-drug screening, J. Natl. Cancer Inst. 82 (1990) 1107–1112, https://doi.org/10.1093/jnci/82.13.1107.
[46] M.C. Alley, D.A. Scudiero, A. Monks, M. Hursey, M.J. Czerwinski, D.L. Fine, B. J. Abbott, J.G. Mayo, R. Shoemaker, M.R. Boyd, Feasibility of Drug Screening with Panels of Human Tumor Cell Lines Using a Microculture Tetrazolium Assay, Cancer Res. 48 (1988) 589–601.
[47] T. Mosmann, Rapid colorimetric assay for cellular growth and survival: Application to proliferation and cytotoxicity assays, J. Immunol. Methods. 65 (1983) 55–63, https://doi.org/10.1016/0022-1759(83)90303-4.
[48] C. Vermes, I.; Haanen, C.; Steffens-Nakken, H.; Reutellingsperger, A novel assay for apoptosis flow cytometric detection of phosphatidylserine expression on early apoptotic cells using fluorescein labelled Annexin V, J. Immunol. Methods. 184 (1995) 39–51. https://doi.org/10.1016/j.physb.2005.01.398.
[49] L. Gong, Y. Tang, R. An, M. Lin, L. Chen, J. Du, RTN1-C mediates cerebral ischemia/reperfusion injury via ER stress and mitochondria-associated apoptosis pathways, Cell Death Dis. 8 (2017), e3080, https://doi.org/10.1038/cddis.2017.465.
[50] M. McTigue, B.W. Murray, J.H. Chen, Y.L. Deng, J. Solowiej, R.S. Kania, Molecular conformations, interactions, and properties associated with drug efficiency and clinical performance among VEGFR TK inhibitors, Proc. Natl. Acad. Sci. U. S. A. 109 (2012) 18281–18289, https://doi.org/10.1073/pnas.1207759109.
[51] PDB RCSB. https://www.rcsb.org/structure/4ASD.
[52] M.F. Tolba, A. Esmat, A.M. Al-Abd, S.S. Azab, A.E. Khalifa, H.A. Mosli, S.Z. Abdel-Rahman, A.B. Abdel-Naim, Caffeic acid phenethyl ester synergistically enhances docetaxel and paclitaxel cytotoxicity in prostate cancer cells, IUBMB Life 65 (2013) 716–729, https://doi.org/10.1002/iub.1188.
[53] M.T.A. Bauer, W. Kirby, J.C. Sherris, Antibiotic susceptibility testing by a standardized single disc method, Am J Clin Pathol. 45 (1966) 149–158.
[54] S. Magaldi, S. Mata-Essayag, C. Hartung De Capriles, C. Perez, M.T. Colella, C. Olaizola, Y. Ontiveros, Well diffusion for antifungal susceptibility testing, Int. J. Infect. Dis. 8 (2004) 39–45, https://doi.org/10.1016/j.ijid.2003.03.002.